Hydrogeology Journal (2019) 27:885–914
https://doi.org/10.1007/s10040-018-1896-x

PAPER

Hydrogeology and geochemistry of a tectonically controlled, deep-seated and semi-fossil aquifer in the Zambezi Region (Namibia)

Roland Bäumle[1] · Thomas Himmelsbach[1] · Ursula Noell[1]

Received: 13 March 2018 / Accepted: 4 November 2018 / Published online: 4 December 2018

Abstract

Recent exploration has revealed that deep-seated and large groundwater reservoirs in Africa's intracontinental basins can be regarded as an additional strategic resource for supply of drinking water. The origin, genesis and recharge of these groundwater reservoirs, however, are still poorly understood. A multidisciplinary approach involving remote sensing, geophysical surveys and hydraulic investigations, as well as hydrochemical and isotope studies, was pursued to gain better insight into the genesis and the potential of a recently discovered lower Kalahari aquifer (LKA) located in the Zambezi Region (Namibia). The study shows that regional tectonic activity associated with the propagation of the Okavango Rift Zone had a tremendous impact on the drainage evolution and hydrogeological setting of the region. Furthermore, there is geomorphological evidence that the LKA—prior to tectonic subsidence and burial—was part of a paleochannel of the upper Zambezi River. Hydraulic continuity could be confirmed by geochemical evolution down the flow path. Cation exchange combined with dissolution of calcite progressively produces alkalinity and sodium and consumes calcium in the north–south direction. Comparison of stable isotope content of the LKA with modern rainfall indicates that the recharge occurred under cooler climate conditions. Analysis of ^{14}C concentrations and $^{36}Cl/Cl$ ratios show that the age of the groundwater exceeds 100 ka and is hence older than presumed. It is concluded that the assessment of the sedimentology, tectonic structures and geochemistry are key factors for understanding both the paleoclimatic and modern recharge processes of deep-seated aquifer systems.

Keywords Semi-fossil groundwater · Paleohydrology · Groundwater age · Conceptual models · Namibia · Sub-Saharan Africa

Introduction

Intracontinental basins often comprise significant and partially unexplored fossil or semi-fossil aquifers. Due to their frequently considerable size, large amounts of freshwater are stored in these deep-seated sedimentary aquifers. These aquifers provide a valuable additional source of drinking water, which may be used for industrial and agricultural purposes. Hence, deep-seated aquifers are of increasing relevance to water supply in arid and semi-arid regions of the world. The groundwater, however, is often of considerable age, and the hydrogeology, as well as the exploration potential and recharge processes of such deep-lying groundwater bodies, is poorly understood. Consequently, any ill-considered groundwater extraction can rapidly lead to permanent depletion of aquifer reserves, i.e. groundwater mining (Margat et al. 2006).

In northern Africa, scientific attention was drawn toward aquifers in extensive basins bordering the Sahara Desert to the north, east and south, including the North-Western Sahara Aquifer System (Sahara and Sahel Observatory (OSS) 2008b; Siegfried 2004), the Nubian Aquifer (Sultan et al. 2007, 2011) and groundwater of the Taoudenit (Fontes et al. 1991), and the Illumeden (Sahara and Sahel Observatory (OSS) 2008a) and Lake Chad basins (Bouchez 2015). In southern Africa, the Kalahari Basin was assumed to host several deep-lying sedimentary aquifers. This basin stretches over some 2200 km in a north–south direction from the SE tip of the Democratic Republic of Congo to South Africa, covering a total area of approximately 1.6 million km^2 (Haddon and

✉ Roland Bäumle
Roland.Baeumle@bgr.de

Thomas Himmelsbach
Thomas.Himmelsbach@bgr.de

Ursula Noell
Ursula.Noell@bgr.de

[1] Bundesanstalt für Geowissenschaften und Rohstoffe, Stilleweg 2, 30655 Hannover, Germany

McCarthy 2005). In the Northern Kalahari, here defined as the area to the north of the Proterozoic Ghanzi–Chobe orogenic belt (Fig. 1a), sedimentary depocenters with thickness exceeding 400 m are developed in the border area between Angola and Namibia and in the Okavango Rift Zone (ORZ) (Haddon 2005; Miller et al. 2010). In these areas, two deep-seated freshwater aquifers were discovered in recent years: the Ohangwena II aquifer (Fig. 1c), which is developed within a paleo-fan of the Cubango River (Lindenmaier et al. 2014; Wallner et al. 2017), and the Lower Kalahari Aquifer (LKA) in the Zambezi Region (ZR) of Namibia, which is the subject of this study. Recent geophysical investigations provide evidence that the Okavango Delta in Botswana is also underlain by a sedimentary freshwater aquifer (Podgorski et al. 2013, 2015). Due to its sedimentological and tectonic position and the prevailing low hydraulic gradients in these basins, the groundwater is considered semi-fossil. This means that the infiltration of water occurred a considerable time ago under wetter climatic conditions (pluvials), but that the aquifer is probably still connected to the hydraulic cycle and replenished to some extent.

The LKA is situated in the eastern parts of the Zambezi Region between 17°30′S and 18°30′S and between 23°15′E and 24°30′E, and is bordered to the east and south by the Kwando and Linyanti rivers, respectively (Fig. 1). Based on exploratory boreholes drilled between 2003 and 2007, the LKA is found at depths from 130 to > 250 m as part of the sedimentary succession of the Kalahari Supergroup (Margane and Beukes 2007). It was recognized during the early stages of investigation that the development of the aquifer system in this area was affected by tectonic subsidence and uplift (Margane et al. 2005). The nature of past and recent recharge, however, remained unclear. The emphasis of the actual study is on the assessment of sedimentology and tectonic evolutions, as they are considered crucial for understanding both the paleoclimatic and the recent recharge processes. An interdisciplinary, stepwise approach was developed involving (i) remote sensing data for the detection of characteristic landforms and lineaments, (ii) geophysical surveys to define the aquifer structure, and (iii) hydraulic, (iv) hydrochemical and (v) isotope studies to assess and characterize hydraulic interactions and flow processes. The study includes a comprehensive review of the literature on the paleoclimatological and geological conditions in the Kalahari Basin.

In the early 1990s, an extensive drilling program for rural water supply was realized (Margane et al. 2005), and subsequent groundwater investigations were carried out at the beginning of the millennium under a bilateral technical cooperation project between Namibia and Germany. All these activities led to a fair amount of reliable hydrogeological information available for the ZR. However, compared to the adjacent Okavango Basin, very few international studies exist in this area.

Fig. 1 **a** Map showing the study area, the position of the Okavango Rift Zone and the presumed maximum extent of paleolakes in the Makgadikgadi Basin. *LKA* = Lower Kalahari Aquifer. **b** Surface topography (vertical exaggeration ≈ 500) and conceptual geological cross section (vertical axis strongly exaggerated and not to scale). **c** Inlay map shows the approximate extent of the Kalahari Basin (after Haddon 2005) and the Kwando-Chobe Catchment. *OKZA* = Okavango–Kalahari–Zimbabwe Axis; *GTA* = Griqualand–Transvaal Axis; *OhR*, *OmR* and *ZR* = Ohangwena, Omaheke and Zambezi regions in Namibia, respectively

Materials and methods

Study area

Hydrology and climate

The catchment of the Kwando-Linyanti-Chobe system, whose headwaters lie in the Angolan highlands, covers an area of over 156,000 km^2 and is situated between 13°S and 19°S and between 19°E and 14°E (Fig. 1a). In the case of rare high floods, the Kwando River is connected to the adjacent endorheic drainage system of the Okavango River via the Magweqgana Spillway (Fig. 2). The source of the Kwando River is located at an elevation of about 1350 m above sea level (a.s.l.). The lowest parts of the catchment are formed by the Linyanti-Chobe floodplains, which lie at about 930–940 m a.s.l., and the adjacent endorheic Mababe (917–930 m a.s.l.) and the Makgadikgadi (900–930 m a.s.l.) depressions. Compared to neighboring rivers, the Kwando at the gauging station in Kongola is characterized by remarkably small average discharge of 31.9 m^3/s, corresponding to 9 mm/a, and relatively low seasonal variation. This is indicative of high evapo-transpiration losses from widespread meanders, oxbow lakes, swamps and floodplains, and of losses during infiltration to the underlying shallow groundwater. This assumption is consistent with measurements of the average annual temperature and class A pan evaporation at the Katima Mulilo (17°30′S, 24°16′E, 946 m a.s.l.) and Sesheke stations (17°28′S, 24°18′E, 944 m a.s.l.) located nearest the study area (Fig. 2), which vary between 21.3 and 21.9 °C and between 2215 and 2506 mm/a, respectively (Margane et al. 2005; Yachiyo Engineering Co. Ltd. 1995).

The climate of the ZR is referred to as a hot arid steppe climate (BSh) by the Köppen-Geiger system (Peel et al. 2007) and is characterized by cool and dry winters, with minimum temperatures during June and July, and a hot rainy season during the summer months from mid-November to March. The rainfall regime is referred to by Gasse et al. (2008) as uni-modal austral summer rainfall. Due to the convective nature of rainfall events, thunderstorms are common, and the rainfall regime shows strong variations from year to year as well as spatial variability. The ZR marks a transition zone between semi-humid and semi-arid conditions, as regional

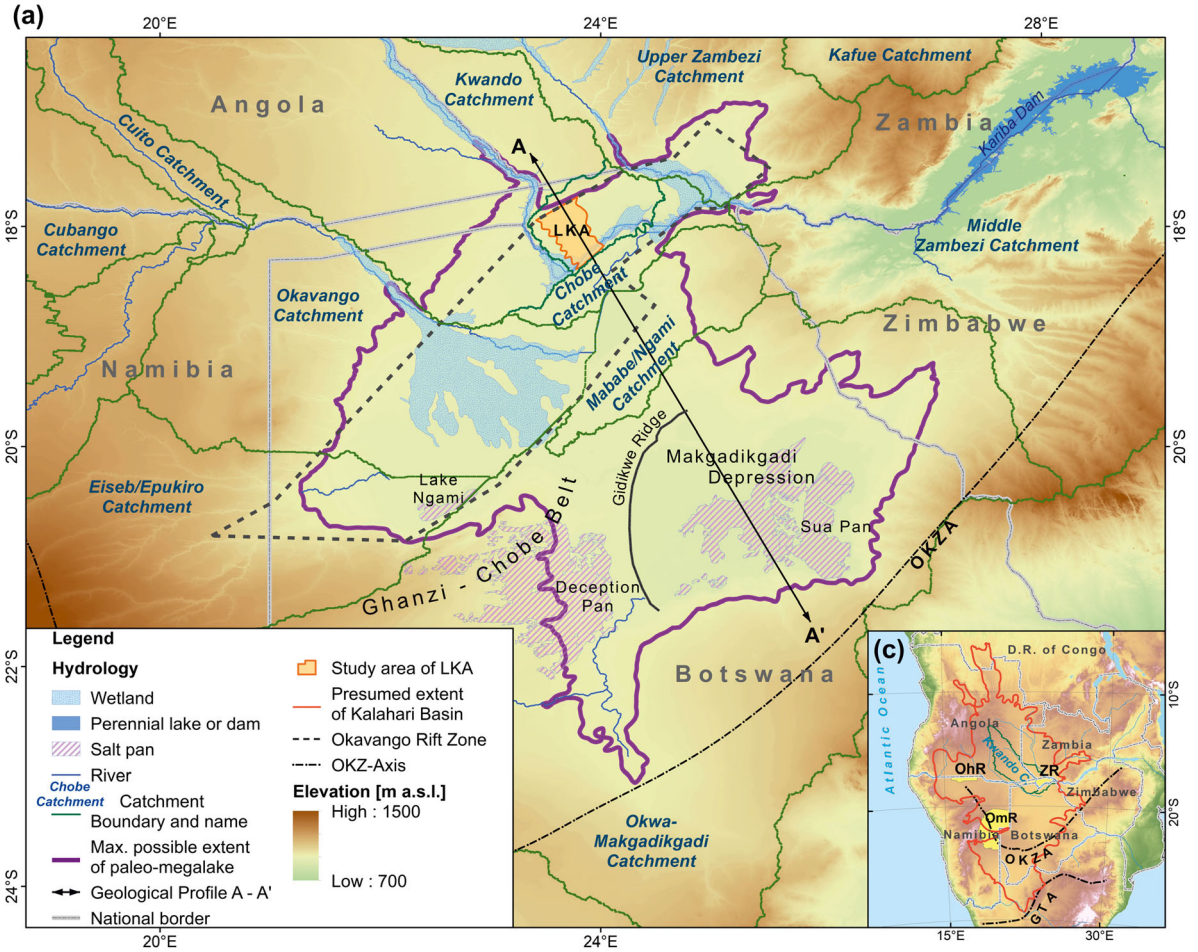
(a)
20°E
24°E
28°E
18°S
20°S
22°S
24°S
Angola
Namibia
Botswana
Zambia
Zimbabwe
Kwando Catchment
Upper Zambezi Catchment
Kafue Catchment
Kariba Dam
Cuito Catchment
Cubango Catchment
Okavango Catchment
LKA
Chobe Catchment
Middle Zambezi Catchment
Mababe/Ngami Catchment
Gidikwe Ridge
Makgadikgadi Depression
Lake Ngami
Sua Pan
Deception Pan
Ghanzi - Chobe Belt
Eiseb/Epukiro Catchment
Okwa-Makgadikgadi Catchment
OKZA
A
A'
Legend
Hydrology
Wetland
Perennial lake or dam
Salt pan
River
Chobe Catchment
Catchment Boundary and name
Max. possible extent of paleo-megalake
Geological Profile A - A'
National border
Study area of LKA
Presumed extent of Kalahari Basin
Okavango Rift Zone
OKZ-Axis
Elevation [m a.s.l.]
High : 1500
Low : 700
(c)
D.R. of Congo
Angola
Zambia
Zimbabwe
Namibia
Botswana
Atlantic Ocean
OhR
ZR
DmR
OKZA
GTA
10°S
20°S
15°E
30°E

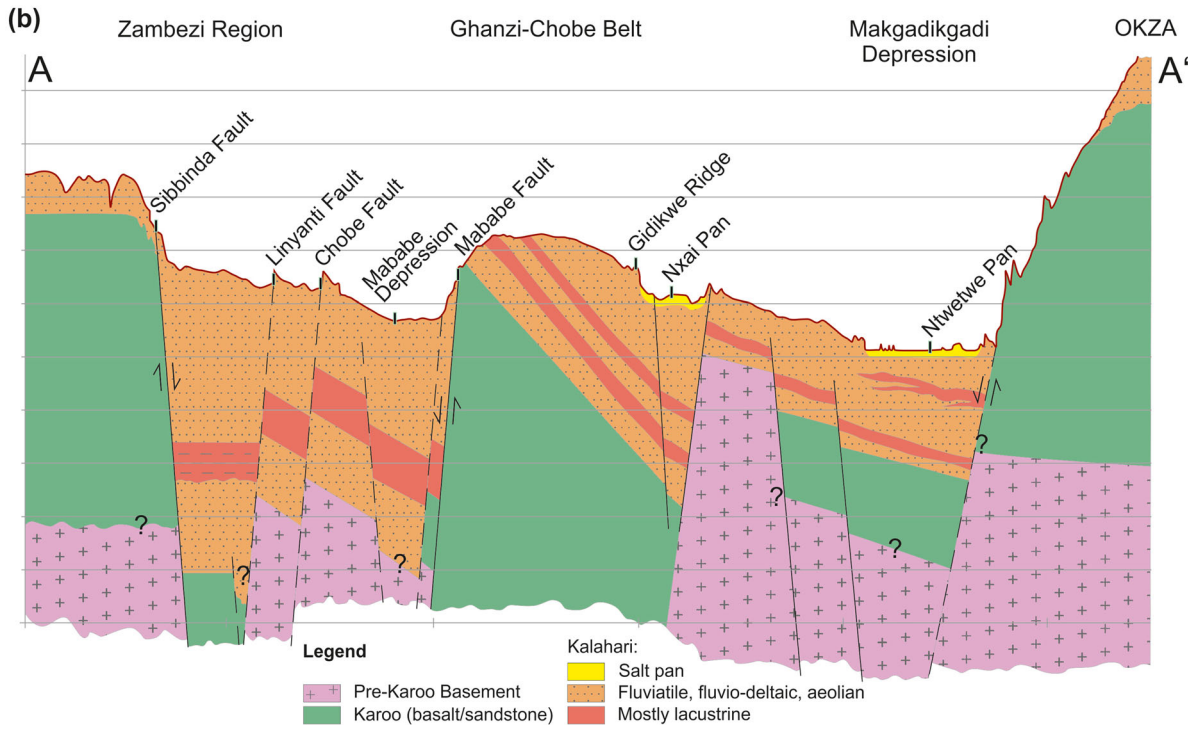
(b)
Zambezi Region
Ghanzi-Chobe Belt
Makgadikgadi Depression
OKZA
A
A'
Sibbinda Fault
Linyanti Fault
Chobe Fault
Mababe Depression
Mababe Fault
Gidikwe Ridge
Nxai Pan
Ntwetwe Pan
Legend
Pre-Karoo Basement
Karoo (basalt/sandstone)
Kalahari:
Salt pan
Fluviatile, fluvio-deltaic, aeolian
Mostly lacustrine

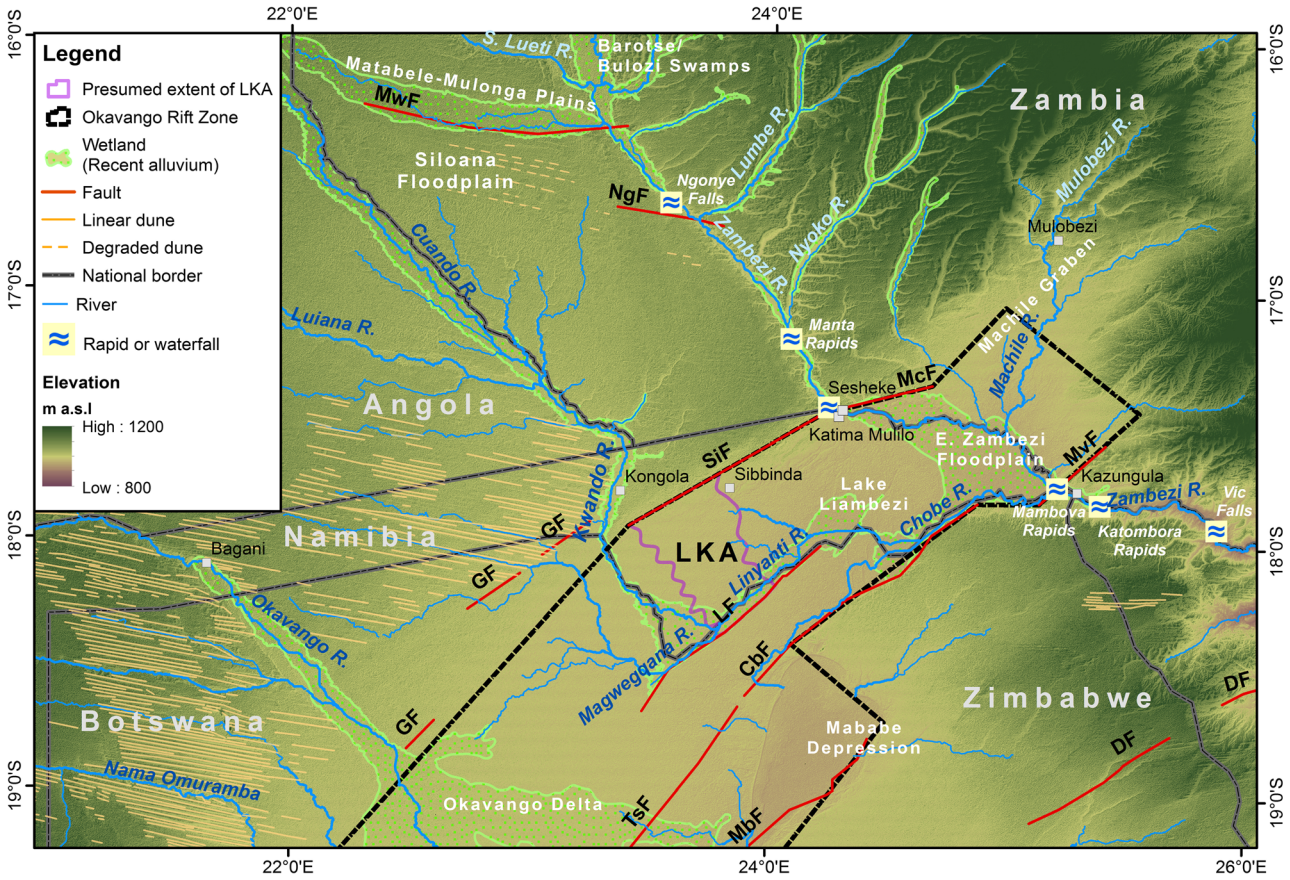

Fig. 2 Elevation, geomorphology and main structural features in ZR and adjacent areas. Faults are abbreviated as follows: *CbF* = Chobe Fault, *DF* = Deka Fault, *GF* = Gumare Fault, *LF* = Linyanti Fault, *MbF* = Mababe Fault, *McF* = Machile Fault, *MvF* = Mambova Fault, *MwF* = Mwamba Fault, *NgF* = Ngonye Fault, *SiF* = Sibbinda Fault, *TsF* = Tsau Fault

precipitation in southwestern Africa is controlled by the seasonal shift of the Intertropical Convergence Zone (ITCZ) and the development of the Congo Air Boundary (CAB). The former marks the surface air boundary between the northeast and (dry) southeast trade winds, the latter between low-level tropical easterlies from the Indian Ocean and westerly unstable and moist air flows from the Congo Basin (e.g. Gasse et al. 2008; Nicholson 2011; Reason et al. 2006). Rainfall in the Northern Kalahari is hence associated with a complex interplay of airstreams originating from the warm western Indian Ocean and the South Atlantic off the northern Angolan and Congolese coastline. In contrast, the Atlantic coastline south of approximately 16°S is influenced by the Benguela Upwelling system of cold water, which stabilizes air and prevents convection throughout the year. The cold sea surface temperatures are therefore the reason for the pronounced aridity along the Namibian and southern Angolan coastlines.

The highest mean annual rainfall (MAR) in the region is observed in the Angolan highlands, with maximum values for the upper Okavango and Kwando river catchments of about 1200–1400 mm/a (Pombo et al. 2015; Steudel et al. 2013), whilst rainfall in the lowest areas of the basin—the Makgadikgadi Plains—is only 300–400 mm/a (Burrough et al. 2009; Robertson 2004). The MAR at the meteorological stations at Katima Mulilo and Sesheke is 650–700 mm, with 90% occurring during austral summer.

Geology and tectonics

Tectonically, the ZR forms part of the ORZ which has been described as an incipient or nascent continental rift basin (Modisi 2000; Modisi et al. 2000) that underwent early stages of continental extension. Continued seismicity in the area provides evidence for ongoing weak tectonic activity in the region (Hutchins et al. 1976; McCarthy 2013; Reeves 1972), which is linked to the propagation of the East African Rift System (EARS) (Bufford et al. 2012). The ORZ forms part of the southwestern branch of the EARS (Modisi et al. 2000), and is defined by three characteristic "en échelon" northeast-trending and probably syntectonic depocenters that correspond to about 100-km-long and 40–80-km-wide structural graben systems, namely the Ngami, Mababe and the Linyanti-Chobe depressions (Kinabo et al. 2007). In total, this complex graben and horst structure is about 450 km long and

150 km wide (Fig. 1a). In the northeastern direction, the ORZ borders the Machile Basin, which also represents a graben structure and once formed the valley of the proto-Kafue River (Moore et al. 2013). Wanke (2005) determined from Landsat TM images that the Eiseb Graben in the Omaheke Region (Fig. 1c) in eastern Namibia represents a southeastward extension of the ORZ.

The depressions are filled with predominantly fluviatile-lacustrine deposits of the Kalahari Supergroup. The Kalahari Supergroup is an Upper Cretaceous to recent sedimentary succession consisting of terrestrial, siliciclastic, unconsolidated to semi-consolidated sediments overlying basement rocks. The sediments are composed mainly of conglomerates, gravels, clays, sandstones and unconsolidated sands. The base of the Kalahari corresponds to the Cretaceous African (Erosion) Surface, which was described by Miller (2008) as a "deeply dissected pre-Kalahari terrain". The interior basin developed in response to "downwarp" and epeirogenic uplift along several axes including the Okavango–Kalahari–Zimbabwe Axis (OKZA) during the Upper Cretaceous/Early Tertiary (de Wit 2007; Haddon and McCarthy 2005). Epeirogenic uplift alternated with extended episodes of tectonic stability and erosion. Hence, deposition was intermittent, with periods of non-deposition corresponding to pedogenetic phases and phases of pedogenetic cementation (Miller 2008). It is generally assumed that the unconsolidated sand in the Kalahari Basin was formed either by fluvial or aeolian transport of material or by weathering of in situ sandstones, and that both processes occurred simultaneously (Gärtner et al. 2013; Haddon 2005).

The Kalahari Group is commonly underlain by basalts of the Karoo Supergroup which are allocated to the Batoka, Stormberg or Rundu formations in Zambia, Botswana/Zimbabwe and Namibia, respectively. The Karoo basalts erupted mainly between 184 and 178 Ma (Jourdan et al. 2005, 2007; Jones et al. 2001 and ref. therein). Money (1972) and Ridgway and Money (1981) describe the Batoka Basalt in western Zambia as an often olivine-rich tholeiite. In the Barotse Basin of Zambia, the thickness of the basalts increases in the western direction, from 30 m at the eastern margin to a maximum observed thickness of 390 m in the south along the Zambezi River (Unrug 1987). In Botswana, the basalts are up to 1000 m thick (Key and Ayres 2000). Surface outcrops of basalt are present over a large area in the Zambezi valley upstream and below the Victoria Falls. Smaller outcrops form the rapids in the upper course of the Zambezi River, e.g. Ngonye Falls and Mambova Rapids (Fig. 2). Interpretation of aeromagnetic data shows that basalt suboutcrops are widespread throughout northeastern Namibia (Fig. 16.4a in Miller 2008) as well as in northern Botswana (Key and Mothibi 1999).

Hydrogeology

A continuous aquifer, referred to as the Upper Kalahari Aquifer (UKA), which is characterized by Quaternary unconsolidated sand and silt of the Kalahari Supergroup, covers the entire area of the ORZ. The mainly alluvial deposits can be divided into recent and older alluvium (Thomas and Shaw 1991). The recent alluvium is seasonally inundated by the Okavango, Kwando, Linyanti, Chobe and Zambezi floodwaters and represents the riverine floodplains of the Okavango Delta, the Kwando River, the Linyanti-Chobe swamps and the Eastern Zambezi Floodplains (Fig. 2). Older alluvium covering the remaining areas, in contrast, is characterized by virtual absence of modern surface discharge. Areas to the north and northwest of the ORZ, i.e. west of the Kwando River, are largely covered by ancient linear dune fields (O'Connor and Thomas 1999; Thomas et al. 2000), being part of the large Northern Kalahari Dune Field (Stokes et al. 1998). In the ZR, elevated areas to the north of the Kongola-Katima Mulilo Highway (Fig. 2) are covered by alluvial sand or reworked aeolian sand. The vegetation is dominated by Kalahari, miombo and teak woodlands, which are deep-rooting trees (Fanshawe 2010). The older alluvium to the south is entirely different and has been described as abandoned inland fans that are covered by loamy soils and dominated by mopane woodland (Baars 1996; Mendelsohn and Roberts 1997). Mopane trees are essentially shallow rooters and are known to be more salt-tolerant than most other savanna tree species. They are therefore indicative of higher clay content and poorly drained and often alkaline soils.

The LKA was discovered by means of exploratory drilling carried out between 2004 and 2007. Five boreholes were drilled into the LKA. The top of the LKA was identified at depths between 125 and 150 m (Margane et al. 2005; Margane and Beukes 2007). In the two northern locations (boreholes no. 041002 and 041004), the Karoo basalts were found to underlie the Kalahari at depths between 193 and 222 m. For the two boreholes no. 041006 and 200254 (Fig. 3) drilled further south, the base of the Kalahari was not reached at the final drilling depth of 189 m and 250 m, respectively. The sediments of the LKA are made of fine- to medium-grained sandstones with interbedded layers of clay and calcareous or silicified sandstone. The LKA appears to be hydraulically separated from the upper aquifer by a bluish-green layer of clay or clayey silt with sand, which in large parts of the area forms a continuous, low-permeable layer. Between 2007 and 2015, 16 additional boreholes with depths varying from 130 to 250 m were established to provide water for small settlements or cattle stations. Unfortunately, detailed lithological and hydraulic records for these boreholes are not available. In contrast to the UKA, the groundwater of the LKA is mostly fresh.

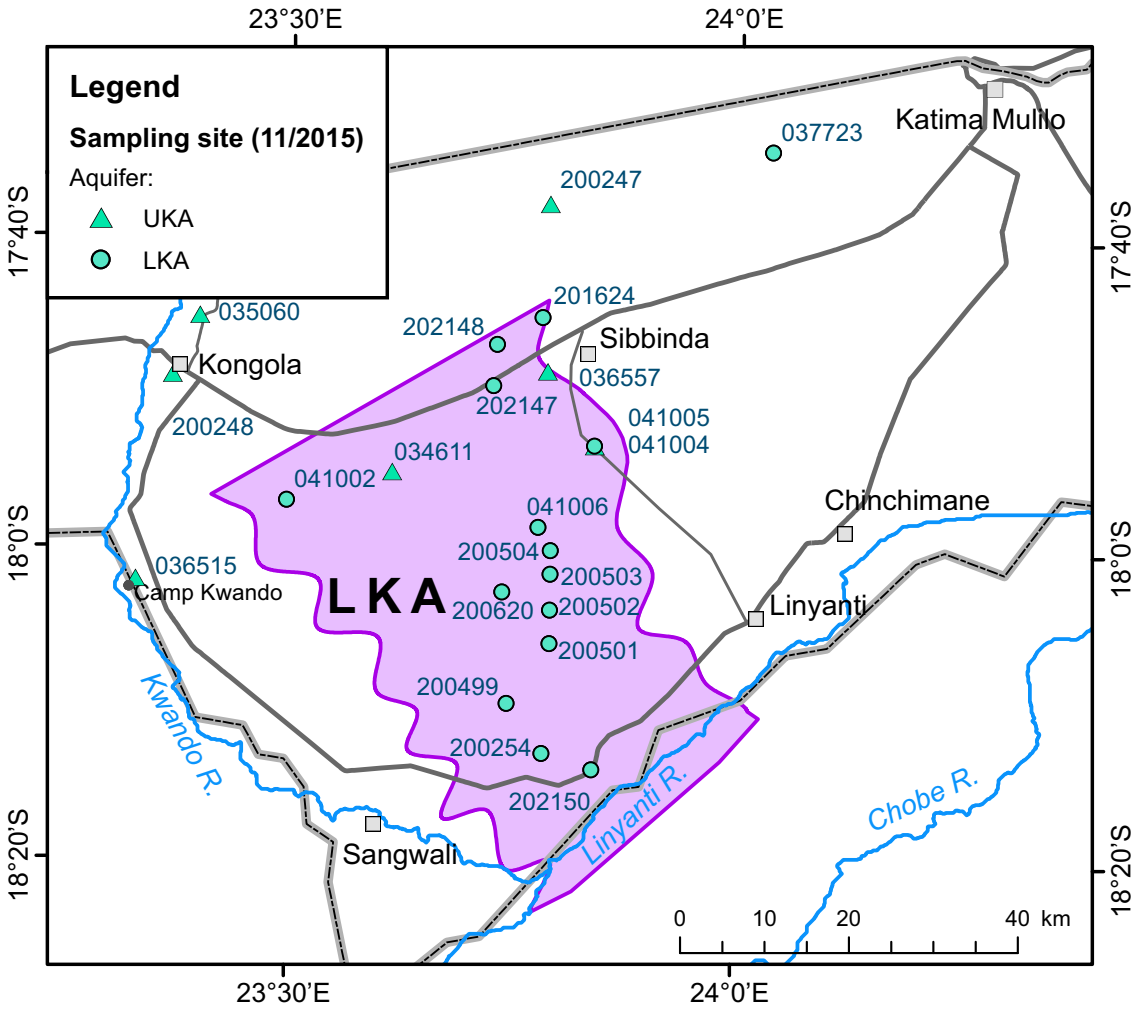

Fig. 3 Sampling points and presumed limits of the LKA

Paleo-drainage conditions

As the Kalahari Basin undergoes tectonic deformation, there is a strong structural control on its drainage network. It is nowadays generally assumed that the Limpopo River was the main river draining the central interior areas of southern Africa, and that the Okavango, Kwando, upper Zambezi, Kafue and Luangwa rivers formed part of this enormous paleo-drainage basin (Moore 2004; Moore and Larkin 2001). Flow of these northern tributaries into the Limpopo River was severed by downwarp of the Kalahari Basin and epeirogenic uplift along the OKZA and the Griqualand–Transvaal Axis, located further south. The OKZA thus broadly forms the divide between the endorheic parts of the northern Kalahari Basin and the Limpopo and Orange rivers. The timing of the uplift and formation of the endorheic interior drainage basin is uncertain, but the Late Cretaceous (c. 65 Ma) has been suggested as an upper constraint. A late Paleogene age (c. 25 Ma) may, however, be much more realistic. Several distinct phases of rejuvenation of uplift along these axes occurred during the Late Oligocene (c. 24–20 Ma), Late Miocene (c. 10 Ma) and Pliocene (Haddon 2005; Walford et al. 2005).

Abrupt changes in river courses are numerous in the area and are often interpreted as capture elbows formed by tectonic movements, changes in base levels and subsequent headward erosion. Tectonic movement also led to the formation of paleolakes of varying size covering the Makgadikgadi Basin and adjacent areas such as today's Okavango Delta and the ZR. Nugent (1990) recognized that the Upper Zambezi and the Mid-Zambezi system, which is located downstream of Victoria Falls, developed as separate rivers until comparatively recent times. Cotterill (2006) and subsequently Moore et al. (2013) suggested that uplift along the Chobe Fault associated with the propagation of the EARS has blocked the flow of the Upper Zambezi (then still the receiving water of the Chambeshi and Kafue rivers) into the Mid-Zambezi. Thus, the river

was diverted into the Makgadikgadi Basin. Basalt bars exposed at the Katombora and Mambova rapids are believed to represent faulted blocks of the Chobe and Linyanti horst, respectively, and mark the points behind which a large paleolake was impounded. As a result of the drainage evolution of the Okavango-Kwando-Zambezi river system, a characteristic distribution of older and recent alluvial and lacustrine sediments has developed, stretching in the NE–SW direction across the ORZ (Moore and Larkin 2001; Thomas and Shaw 1991) and often confined by faults and dune fields (McCarthy 2013). Drainage evolution models developed by Cotterill (2006) and Moore et al. (2013) suggest that the age of large paleolakes in the area exceeds 500 ka. The largest lake was named Paleolake Deception (PLD) after a small eastward-flowing ephemeral tributary to the Makgadikgadi Basin and was discovered by McFarlane and Eckardt (2008). It presumably filled the basin to an elevation of 995 m a.s.l. and possibly covered a total area of 173,000 km^2, about 2.5 times the size of Lake Victoria (Fig. 1a). Paleolake Makgadikgadi (PLM) represents the 945-m a.s.l. stage; its extent is clearly visible in aerial photos and satellite images by the Gidikwe Ridge (Fig. 1a), which is interpreted as an offshore barrier bar along the western shoreline of the paleolake. PLM that may have reached a total area of 65,000 km^2 has been extensively described in the literature over the last 50 years (Burrough et al. 2009; Grove 1969; Heine 1987; Meier 2008; Ringrose et al. 2005; Shaw 1988; Thomas and Shaw 1991). Interpretation of helicopter time-domain electromagnetic (HTEM) data provides evidence that PLM extended northeastward into the region presently occupied by the Okavango Delta (Podgorski et al. 2013). A smaller paleolake is associated with an elevation of 930 m a.s.l. and referred to as Paleolake Thamalakane (PLT). Shaw and Thomas (1988) proved the existence of a paleolake in the ZR, which they named Paleolake Caprivi (PLC). The PLC probably corresponds to the PLT stage. This lake was originally believed to have existed until fairly recent times, but the results of the radiocarbon dating of shoreline Mollusca which suggested at least two lake stages at 15 and 2–3 ka BP are now considered incorrect (e.g. Moore 2004) due to the fact that carbon samples are often contaminated by modern or old ("dead") inorganic carbon.

The sudden change in the flow direction of the Kwando River along the border between Namibia and Botswana is obviously related to tectonic uplift along the Linyanti Fault (Fig. 2). Thus, the change in flow from a southern to eastern direction must be understood as a tectonically driven river diversion rather than capture by headward erosion (Moore 2004). Sand spits at the eastern shoreline of the Sowa (formerly Sua) Pan (eastern Makgadikgadi Pan, Fig. 2) were interpreted as relict fluvial channels of the former Kwando River before its flow was diverted (Moore and Larkin 2001). This indicates that the flow of the Kwando was directed to the south into the Makgadikgadi depression prior to tectonism related to the propagation of the EARS.

Paleoclimate

It is generally recognized that, despite some notable interruptions, the western, northern (Sahara-Sahel) and eastern regions in Africa experienced overall warmer conditions and above-average rainfall during the Early to Mid-Holocene, which corresponds to a warm interglacial. The interval is known as the African Humid Period (AHP), lasting—depending on the author—from 14.8–11.0 ka to 5.5–4.0 ka calibrated years before the present (cal. BP) (e.g. deMenocal et al. 2000; Gasse 2000; Willis et al. 2013 and ref. therein). The warmer and wetter conditions have been linked to a northward migration of the ITCZ due to an increased, partially orbitally driven interhemispheric insolation contrast and an intensification of the African monsoon. Cooler tropical temperatures and more arid conditions persisted throughout northern and most of East Africa during the Last Glacial Maximum (LGM). Various terrestrial records indicate broad arid phases between 23 and 17 ka, and lake levels in Africa were almost uniformly low during the LGM (Feakins and deMenocal 2010 and ref. therein).

The climatic conditions during the LGM and Holocene in the southern rainfall zone, and in particular the Kalahari environment, are more complex and are still a subject of controversy. This may be attributed to the extreme climate variability of the Kalahari Basin due to its position between a tropical summer rainfall and temperate winter rainfall regime, the scarcity of terrigenous proxies in arid climates and difficulties inherent in the various available dating technologies. There is generally good agreement that colder temperatures prevailed in southern Africa during the LGM, and that the winter rainfall zone expanded northward and experienced wetter conditions (Chase and Meadows 2007). Noble gas temperature records from the Stampriet Artesian Basin south of Windhoek (24°S, 19.5°E) and from a southeastern Kalahari aquifer near Letlhakeng, Botswana (24.1°S, 25°E) suggest that temperatures during the LGM were lower than today by 5–6 °C (Kulongoski et al. 2004; Stute and Talma 1997). According to Stute and Talma (1997), higher than expected $\delta^{18}O$ values in groundwater provide evidence that the Stampriet area, which is today under the influence of rainfall originating largely from the Indian Ocean, may have received more Atlantic moisture during the LGM due to a northward shift of the winter rainfall zone. The dominant influence of the migration of tropical and subtropical circulation features on climate variability in southern Africa has been widely emphasized (Stone 2014). A conceptual climate model suggests that during interglacials, warming of the Northern Hemisphere

(NH)—as the hemisphere with more land—is accentuated, which results in an overall northward shift of the ITCZ. For the African continent, this leads to increased rainfall over subtropical northern Africa (as during the AHP) and to a decrease in precipitation in the summer rainfall region (Chiang and Friedman 2012; Railsback 2017; Schneider et al. 2014). Conversely, due to the glaciation over the NH, and since the Southern Hemisphere (SH) has the larger fraction of ocean, cooling over the NH during glacial periods is stronger, which pushes the ITCZ southward into the SH. This results in increased aridity of the Sahara-Sahel zone (as during the LGM) and potentially higher rainfall in southern African regions, whereas intermediate conditions presumably prevailed during cooler interglacial periods. This conceptual model of climate change thus underpins the observation that climate variation patterns in northern Africa are very different from those in the SH (e.g. Gasse 2000; McCarthy and Rubidge 2005). The best evidence of this conceptual model predicting insolation-driven increased rainfall over the southern interior during glacial periods is provided by recent studies on sediment cores off the mouth of the Zambezi River (Schefuss et al. 2011; van der Lubbe et al. 2014, 2016), in contrast to comprehensive but partially contradictory results from thermoluminescence (TL) or optically stimulated luminescence (OSL) dating techniques performed on dune sands (Ivester et al. 2010; Munyikwa et al. 2000; O'Connor and Thomas 1999; Stokes et al. 1997a, b; Thomas et al. 2000, 2003). The linear dune fields are widely considered to represent the oldest morphological landforms in the northern Kalahari Basin (McCarthy 2013). Chronological reconstruction of geomorphological events suggest that the dunes are older than 2 Ma (Moore et al. 2013). This is particular obvious in the area southwest of the Okavango Delta where the Gumare Fault (Fig. 2) truncates the east–west-trending dunes. To the east of the Gumare Fault, the dune field has been completely destroyed by flooding, which is a clear indication that the formation of the dunes predates faulting as well as flooding by the development of the mega-paleolakes in the Makgadikgadi subbasin (McFarlane and Eckardt 2007). The determined younger ages of dune sands may be partially explained by dune degradation, bioturbation and overturning, as highlighted by McFarlane et al. (2005); it is plausible that older sands were temporarily exposed to sunlight and subsequently buried again.

Controversy also exists about the development and age of large paleolakes in the Makgadikgadi Basin which were associated with wet phases. A number of studies from the Lake Ngami, Mababe and Makgadikgadi basins that applied OSL and radiocarbon dating methods provide evidence that at least seven paleolake full phases may have occurred in the Makgadikgadi Basin during the late Pleistocene and Holocene (Burrough and Thomas 2008; Burrough et al. 2007, 2009; Gamrod 2009; Ringrose et al. 2005; Shaw et al. 1997). Moore et al. (2013), however, using water budget estimates, showed that the paleolake in the Makgadikgadi Basin could only reach the level of Gidikwe ridge (i.e. the PLM stage) if the Okavango, Upper Zambezi and Kwando rivers all terminated in the Makgadikgadi Basin. Models suggesting that paleolake levels were controlled by major tectonic events rather than climate variations are therefore more convincing and plausible. Moore et al. (2013) proposed that large paleolakes only existed >500 ka years ago in the basin and that they stepwise desiccated after major tributaries of the Upper Zambezi paleo-river system were cut off by tectonic subsidence and lifting and resulting processes such as headward erosion and river capturing.

Remote sensing

A digital elevation model was applied to identify characteristic landforms including dune fields, river fans and terraces, and faults and stream lineaments in the project area. The model uses high-resolution topographic global elevation data generated from NASA's Shuttle Radar Topography Mission (SRTM). The raster data were downloaded from the U.S. Geological Survey's EarthExplorer website (USGS 2015) on 22 January 2015, and have a resolution of 1 arcsecond, or about 30 m × 30 m. In addition, a true-color image dated 8 August 2017, delivered by the European Space Agency's Sentinel-2 satellite mission, was also obtained from the USGS EarthExplorer website (USGS 2017). The RGB (red, green, blue) composite image was created from bands 4, 3, and 2 and has a resolution of 10 m × 10 m.

Geophysical survey

During the years 2003/2004, about 57 transient electromagnetic (TEM) soundings were collected in the ZR. In 2004/2005, the survey was supplemented by an additional 17 soundings in order to extend survey lines toward the north and west (Fielitz et al. 2004). Poseidon Geophysics (Pty) Ltd., Gaborone, collected these soundings as part of the Namibian-German Technical cooperation Project "Investigation of Groundwater Resources and Airborne Geophysical Investigation of Selected Mineral Targets in Namibia".

The TEM soundings were collected using a GDP-32 receiver and a TEM/3 receiver coil (single-channel magnetic antenna) with an effective coil area of 10,000 m^2. In-loop configuration was applied. The transmitter coil was 200 m × 200 m, single-turn, and a GGT-10 transmitter was used. All equipment was supplied by Zonge International (Zonge 2018). In order to achieve investigation depths of some 200 m, the measurements were performed applying 20 A for 1 Hz, 15 A for 4 Hz, and 5 A for 16 Hz—the lower the frequency, the longer the transient and the deeper the investigation depth. The measurements were stacked and averaged, 64 cycles for 1 Hz, 256 cycles for 4 Hz, and 512 cycles for

16 Hz. Standard processing software by Zonge (SHRED, TEMAVG) was used for stacking, averaging and visualization of the data. For data inversion, the TEMIX Plus software program (Interpex Limited, Interpex 2016) was used, and a 1-D inversion was applied.

The soundings were positioned along 16 profiles, partly crossing each other, and with irregular spacing between the soundings. The location of the soundings was aimed at covering the supposed area of the deep freshwater aquifer including its borders. The data quality was very satisfactory. In most cases, it was possible to collect transients up to 20 ms and longer, with low noise. At some locations, the transients collected during the first and the supplementary campaign differed. The detected resistivity shift could not be attributed to technical causes and was considered a reflection of the geological heterogeneity close to the northern graben structure, where most of the supplementary measurements were located.

Investigations of groundwater hydraulics

Groundwater contours for the UKA are based on water table data obtained from the database of the Namibian Department of Water Affairs and Forestry (DWAF). The water table measurements were converted into piezometric heads using elevations obtained from SRTM imagery (1 arcsec or approx. 30 m × 30 m, see Chapter 2.2). The dataset comprised about 750 values for water tables that were taken between 1970 and 2015 during different seasons, i.e. rainy or dry season. Variogram analysis and universal kriging with linear drift was applied for regionalization of water level data and mapping of groundwater contours. In order to construct groundwater contours for the LKA, 16 water table measurements were taken during the end of the dry season from 10 to 23 November 2015. Another nine older water table measurements were added from the database. Contours had to be constructed manually, as kriging or another interpolation method proved unsuccessful due to the limited number and quality of data.

In addition, results from pumping test analyses were statistically examined. Previous pumping test results were reported by Margane and Bäumle (2004) and Margane and Beukes (2007). Additional test data from the DWAF archives were analyzed. Finally, the initial, pumped and residual water levels were measured manually and continuously recorded with pressure probes during the sampling campaign conducted in November 2015. The results allowed for rudimentary test pumping analysis. In total, 42 single-well pumping tests from 35 boreholes were able to be analyzed: 20 for the UKA and 22 for the LKA. Pumping duration ranged from 1 to 72 h, and pumping rates also varied widely, from 0.2 to 58 l/s.

Sampling and analytical procedures

Groundwater samples from 22 boreholes were obtained during the field campaign carried out in November 2015. The bulk of groundwater samples were taken along a north–south-directed transect at around 23°45′E (Fig. 3). The boreholes are mostly used for providing drinking water or water for stock in cattle camps, and are installed with a submersible pump or in lesser cases with a hand pump. Five of the sampled boreholes are used as monitoring wells by DWAF and are thus permanently equipped with data loggers. Except for the monitoring boreholes, completion reports containing a detailed lithological description were not always available. It was hence difficult to determine with certainty the position of the confining unit separating the LKA from the UKA. It was deduced from this that boreholes with depths exceeding 130 m could potentially tap the LKA. Fifteen of the 21 sampled boreholes fulfilled this depth criteria (maximum depth 250 m). It should be noted that for boreholes 037223, 200501, 200503, 200504 and 200620, the position of the screens is unknown, and that for boreholes 202147, 202148 and possibly 201624, the upper parts of the screens are located within the UKA (Appendix Table 2). During this and two previous campaigns, a number of additional samples were taken from boreholes of the UKA and the Kwando River, as well as from a PVC rainfall collector that was set up at Camp Kwando Lodge (23°19′E, 18°03′S, 963 m a.s.l.), about 25 km south of Kongola Bridge, for purposes of comparison.

Physicochemical parameters were measured using commercial portable meters (WTW/Xylem Group) as part of through-flow cells to avoid any contact of groundwater with atmospheric oxygen and carbon dioxide. In situ measurements included temperature (T), electrical conductivity (EC), pH, dissolved oxygen (DO) and oxidation-reduction potential (Eh)(measured against an Ag/AgCl electrode and corrected with respect to standard hydrogen electrode). The pump rate was measured volumetrically using a 20-l container and a stopwatch. Alkalinity and acidity were determined onsite by potentiometric titration on 100-ml unfiltered samples using a field burette. The normality of the titrant solutions (HCl, NaOH) was 0.047 N. The titration was considered important, as in previous campaigns it was observed that pH measured in situ was usually higher (more alkaline) than in samples in the laboratory. The lowering of the pH was explained by dissolution of atmospheric CO_2 in the sample water. A fixed-endpoint method (to pH 4.3), and USGS Inflection Point Titration (IPT) and GRAN function plot methods were applied for analysis (Rounds 2012). The data were entered in a customized spreadsheet and preliminarily analyzed on a laptop in the field. The samples were taken once all in situ parameters

except Eh had completely stabilized, which took between 60 and 120 min. Eh values dropped continuously from the start of pumping, but toward the end of pumping, the fluctuations gradually diminished. The submersible pumps yielded pump rates in the range of 0.8 to 1.4 l/s, which resulted in a total abstracted volume of water of between 2 and 8.6 m^3. Much smaller amounts, however, were extracted from boreholes with hand pumps. The samples were continuously kept at low temperature using cooling boxes and frozen cooling elements.

Inorganic components and the stable hydrogen and oxygen isotopes were analyzed by the BGR laboratory in Hannover, Germany. Carbon isotopes and chlorine-36 were analyzed by the external accredited laboratory, Hydroisotop GmbH, in Schweitenkirchen, Germany. The applied analysis methods are summarized in Table 1. The isotopic composition of hydrogen (δ^2H) and oxygen ($\delta^{18}O$) was determined using a Picarro cavity ring-down spectrometer (CRDS) equipped with a CTC autosampler. The measurements were normalized to the Vienna Standard Mean Ocean Water/Standard Light Atmospheric Precipitation (VSMOW/SLAP) scale, where values of 0 and −428 ‰ for δ^2H and 0 and −55.5 ‰ for $\delta^{18}O$ were assigned to VSMOW and SLAP, respectively. The external reproducibility (standard deviation of a control standard during all runs) was better than ±1.0 ‰ for δ^2H and ±0.1 ‰ for $\delta^{18}O$. The results for $\delta^{18}O$ and δ^2H are expressed in the conventional notation as relative deviations in per mil (‰ or 10^{-3}) from the VSMOW according to the following relationship (Coplen 2011):

$$\delta = 1,000\left(\frac{R_{\text{sample}}}{R_{\text{VSMOW}}}-1\right) \quad (1)$$

where R_{sample} is the isotopic ratio of the sample ($^2H/^1H$ or $^{18}O/^{16}O$) and R_{VSMOW} is the isotopic ratio of the standard.

The deuterium excess D_{ex} is calculated from the isotopic composition of δ^2H and $\delta^{18}O$ as follows:

$$D_{\text{ex}} = \delta^2H - 8\,\delta^{18}O \quad (2)$$

The D_{ex} is about 10 ‰ for rain that plots near the Global Meteoric Water Line (GMWL), but is much lower for surface water and groundwater that have lost some volume to evaporation. The D_{ex} thus serves as a valuable tool for tracing the origin of water.

Carbon-13 (^{13}C) content was determined using isotope ratio mass spectrometry (IRMS). The ^{13}C abundance is reported as the deviation in per mil (‰ or 10^{-3}) of the ratio $^{13}C/^{12}C$ in the sample relative to the $^{13}C/^{12}C$ ratio of the Vienna Pee Dee Belemnite (VPDB) standard, i.e. as $\delta^{13}C$ ‰ VPDB. Measurement reproducibility of duplicates was better than ±0.3 ‰. Carbon-14 (^{14}C) was analyzed using accelerator mass spectrometry (AMS), and ^{14}C activity is given in percent modern carbon (%mC). ^{14}C content expressed in %mC represents the deviation from ^{14}C activity in the undisturbed atmospheric equilibrium that equals 100 %mC or 0.226 Bq/g of carbon. Chlorine-36 (^{36}Cl) is measured as $^{36}Cl/Cl$ ratios and is also determined by AMS. Chloride needs to be extracted from acidified solutions by adding excess $AgNO_3$, resulting in the precipitation of AgCl. Samples with chloride content of less than about 20 mg/L are considered critical, as the mass of precipitated chloride may be insufficient for determining the radioactive isotope ^{36}Cl. Since sulfur concentrations are generally high in the study area, and because the sulfur-36 isotope interferes with ^{36}Cl during AMS analysis, sulfur has to be removed from the samples in an intermediate step. This is achieved by precipitation as $BaSO_4$ (with $Ba(NO_3)_2$) and subsequent removal by centrifugation. The ^{36}Cl concentrations are expressed as 10^{-15} atoms of ^{36}Cl per total atoms of Cl.

Groundwater age dating

Radioactive tracers can be applied to determine the apparent age of groundwater. Radioactive tracers used for the longer timescales are ^{14}C and ^{36}Cl. Both are cosmogenic nuclides, naturally produced in the upper atmosphere from

Table 1 Analysis methods applied

Parameter	Analysis method
Br, Cl, F, NO_2, NO_3, SO_4	Ion chromatography
HCO_3	Titrimetry
NH_4	Photometry
Al, Ba, B, Ca, Fe, K, Mg, Mn, Na, P (PO_4), Si (SiO_2), Sr, Zn	Inductively coupled plasma with optical emission spectroscopy (ICP-OES)
Other metals and trace elements	High-resolution inductively coupled plasma mass spectrometry (HR-ICP-MS)
^2H, ^{18}O	Cavity ring-down spectroscopy (CRDS)
^{13}C	Isotope ratio mass spectrometry (IRMS)
^{14}C, ^{36}Cl	Accelerator mass spectrometry (AMS)

cosmic radiation. For radioactive tracers with known or constant input function, an apparent age can be derived from concentrations using the equation of radioactive decay. Radiocarbon has a half-life of 5730 years, which allows the determination of timescales between some thousand and approximately 35,000 years. ^{36}Cl has a half-life of 301,000 years and is suitable for determining ages on the order of 10^5 to 10^6 years (e.g. Kalin 1999; Phillips 1999; Mook 2000).

Radioactive decay is described by the exponential function:

$$C(t) = C_{re}\exp(-\lambda_t t) \tag{3}$$

where

λ_t is the decay constant of the tracer ($\lambda_{14C} = 1.210{\cdot}10^{-4}a^{-1}$; $\lambda_{36Cl} = 2.303{\cdot}10^{-6}a^{-1}$)
C is the measured tracer concentration of the sample
C_{re} is the (initial) tracer concentration of recharge
t is the time corresponding to the apparent groundwater age

The apparent groundwater age of a sample is calculated as

$$t = \frac{-1}{\lambda_t}\ln\left(\frac{C(t)}{C_{re}}\right) \tag{4}$$

Phillips (2013) described an easy mass balance equation for the absolute ^{36}Cl concentration in an aquifer. The model incorporates radioactive decay of the recharged ^{36}Cl, underground production in the aquifer toward a secular equilibrium ratio of ^{36}Cl /Cl and an additional source of chloride, such as diffusion from an adjacent aquitard, which may have another ^{36}Cl /Cl ratio in secular equilibrium. The Phillips model expressed for the tracer concentration A_{36Cl} as given in Suckow et al. (2016) reads as follows:

$$\begin{aligned} A_{36Cl} = R{\cdot}A_{Cl} = R_{re}A_{Cl,re}\, e^{-\lambda_{36Cl}t} \\ + \left(A_{Cl,re}\, R_{se1} + {}^{F}/_{\lambda_{36Cl}}[R_{se2}-R_{se1}]\right)\left(1-e^{-\lambda_{36Cl}t}\right) \\ + R_{se2}\, F\, t \end{aligned} \tag{5}$$

with

$$F\, t = A_{Cl}-A_{Cl,re} \tag{6}$$

where

A_{36Cl} is the ^{36}Cl concentration [^{36}Cl atoms /L] of the sample
A_{Cl} is the measured Cl^- concentration [Cl^- atoms /L] of the sample
$A_{Cl,re}$ is the recharge concentration [Cl^- atoms /L]
R is the measured ^{36}Cl/Cl ratio (atom:atom) of the sample
R_{re} is the ^{36}Cl/Cl ratio of recharge
R_{se1} is the secular equilibrium ^{36}Cl/Cl ratio in the aquifer
R_{se2} is the secular equilibrium ^{36}Cl/Cl ratio in the adjacent source of Cl (e.g. brine, evaporate, diffusion from aquitard) being added to the system
F $=dA_{Cl}/dt$ is the relative flux of chloride from the aquitard to the aquifer [atoms / (L·year)]

If $R_{se2} = R_{se1}$, the equation simplifies and reads:

$$A_{36Cl} = R \cdot A_{Cl} = (R_{re}{-}R_{se})\, A_{Cl,re}\, e^{-\lambda_{36Cl}t} + R_{se}\,(A_{Cl,re} + F\, t) \tag{7}$$

and the apparent groundwater age is calculated as (Bentley et al. 1986; Phillips et al. 1986)

$$t = \frac{-1}{\lambda_{36Cl}}\ln\frac{A_{Cl}\,(R{-}R_{se})}{A_{Cl,re}\,(R_{re}{-}R_{se})} \tag{8}$$

Furthermore, if chloride is added from dissolution of halite, then $R_{se} = 0$, and consequently (Phillips 2013):

$$A_{36Cl} = R_{re}A_{Cl,re}\, e^{-\lambda_{36Cl}t}, \text{ and } R = \frac{A_{36Cl}}{A_{Cl_{re}} + F\, t} \tag{9}$$

In this case, the equation for apparent groundwater age reads:

$$t = \frac{-1}{\lambda_{36Cl}}\ln\left(\frac{A}{A_{re}}\right) = \frac{-1}{\lambda_{36Cl}}\ln\left(\frac{R{*}Cl}{R_{re}{*}Cl_{re}}\right), \tag{10}$$

where Cl and Cl_{re} represent the measured chloride concentration and the chloride concentration of recharge in mg/L, respectively.

Results

Remote sensing

The high-resolution DEM and true-color image proved suitable for detecting landforms and tectonic regimes in the study area. The Linyanti and Chobe faults are easily detectable in the DEM. The Linyanti fault line located south of the Linyanti River and the Magweqgana Stream is expressed in vertical displacements on the surface of about 4–8 m. Paleolakes likely existed several times in the down-faulted areas north of the Linyanti and Chobe faults. Lake Liambezi (Fig. 2), which episodically fills up after extreme flooding, can be regarded as a remnant of these paleolakes. The Sibbinda Fault to the north marks the boundary of a zone of gradually rising elevation and is considered a blind fault. The elevation south of the fault line is about 970 m above mean sea level (a.s.l.), whereas the plateau north of the fault reaches values well above 1000 m a.s.l. (Fig. 2).

The Kwando and Zambezi rivers have deposited fans into the ORZ similar to but smaller than the Okavango Delta to the southwest (Fig. 4). These fans were also recently discovered from digital elevation data by Burke and Wilkinson (2016). The Kwando Fan and parts of the Zambezi Fan are essentially inactive, because its formative rivers have incised into the relict fan deposits. The fans therefore form the upper part of the older alluvium. Figure 4 also illustrates the strong tectonic control on the drainage system in the study area. Apart from the obvious elbow-shaped river diversion near the Linyanti Fault, the course of the Kwando River is also deflected south of the Matabele-Mulonga Plains and north and south of Kongola. The Matabele-Mulonga Plains, in fact, are believed to represent an abandoned arm of the Kwando River, which hence initially joined the Zambezi in the area of the Barotse-Bulozi Floodplains (Moore et al. 2013). The near-parallel course of the Kwando and Upper Zambezi rivers, as well as the course of the eastern tributaries to the Zambezi such as the Lumbe and Njoko rivers, is also most likely an expression of the regional tectonic setting. The Ngonye Falls near Sioma provide evidence that the section of the

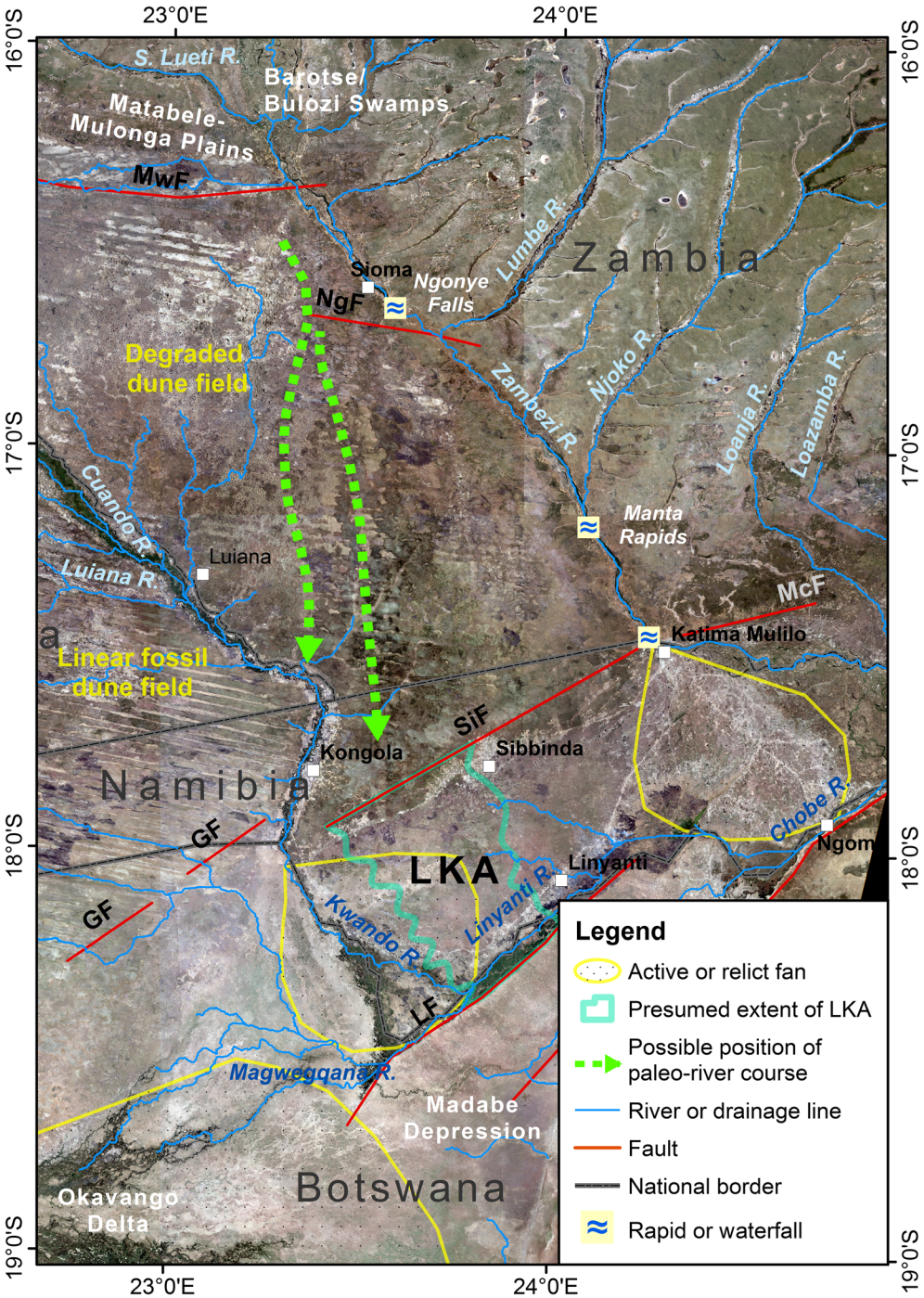

Fig. 4 Prominent landforms in the border area between Angola, Namibia, Botswana and Zambia as seen from a Sentinel-2 RGB composite image mosaic taken on 8 August 2017; abbreviations of faults as in Fig. 2

Zambezi River downstream of the falls is a relatively young valley. The rapids are a clear sign of rejuvenation of an otherwise very mature longitudinal river profile. The Zambezi obviously once followed a route to the west of its modern course crossing the Siloana Floodplain, as indicated by the arrows in Fig. 4. Dune fields in the Northern Kalahari generally developed to the west of large river valleys which supplied the sands for dune formation. To the west of the Kwando and Okavango rivers, linear dune fields are well preserved. The fact that the Siloana Floodplain—in contrast—is characterized by largely degraded dunes and areas without remnant dunes is another indication that the area has undergone extensive fluvial reworking.

Geophysics

The supplementary TEM measurements revealed the boundaries of the alluvial aquifer system toward the east and north (Fig. 5). The basalt appears at sounding 4_16 at profile 9, at sounding 1_200 at profile 1 and at sounding 3_50 at profile 3. All soundings north/west and north along these profiles show the indication of high-resistive basalt (Fig. 5c). The TEM inversion results show a decrease in resistivity toward the alluvial basin. Along profile 9, the basalt dips toward the southeast, from about 20 m depth at sounding 4_08 to about 100 m depth at sounding 4_16.

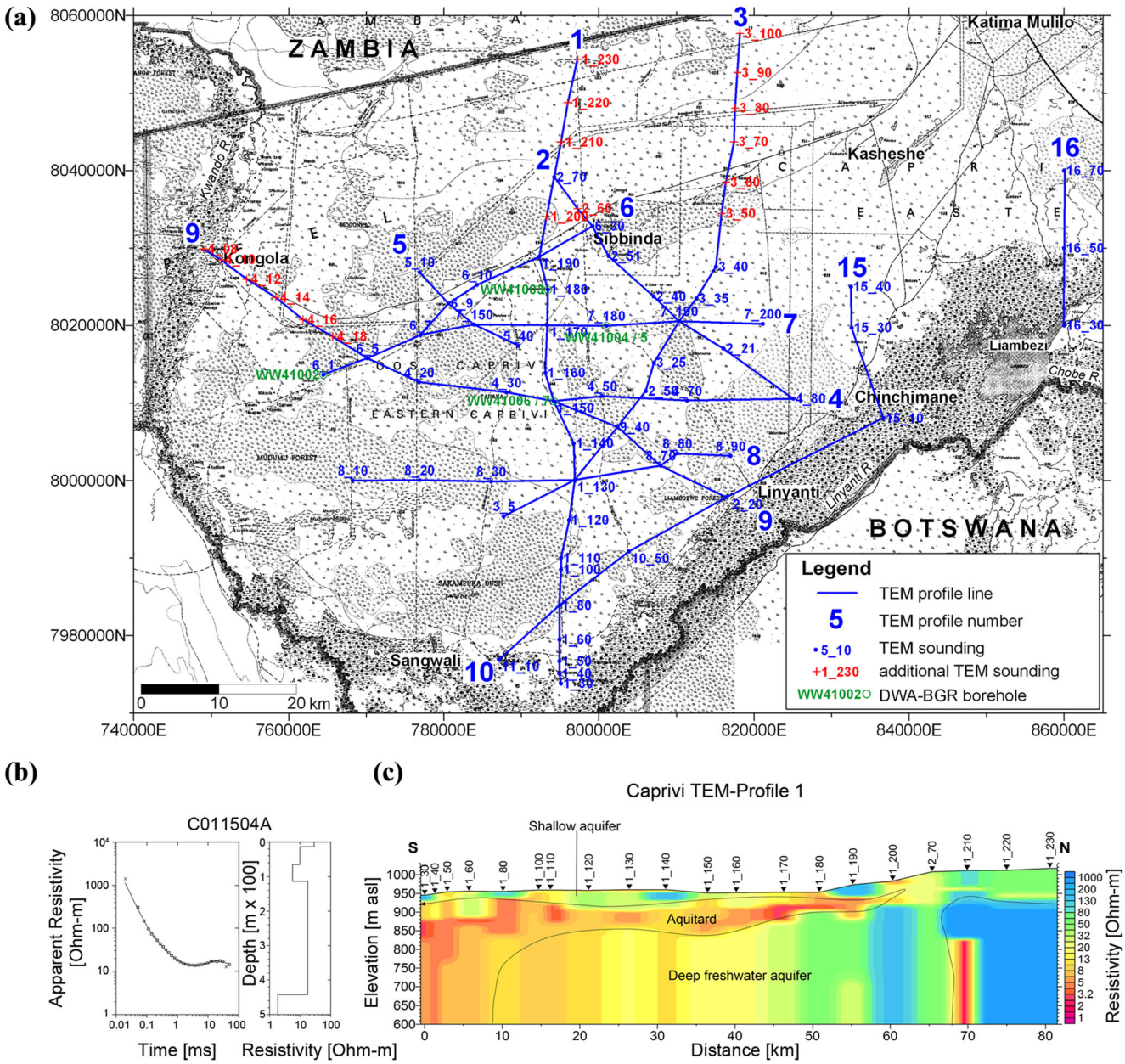

Fig. 5 **a** Location of the TEM soundings and profiles. **b** Left: characteristic TEM sounding curve recalculated into resistivity with late time approximation (sounding 1_ 150). Right: model from the 1-D data inversion. **c** TEM 1-D inversion results for profile 1

The alluvial filling, with its relatively low resistivity of some 20 Ωm, is clearly seen from sounding 4_20 toward the southeast. From sounding 4_08 to sounding 6_5, the resistivity of the basalt layer drops from about 1000 Ωm at 4_08 to some 50 Ωm at 6_5.

At the southern end of the TEM profiles, no indication of higher resistivity at depth is detected. In Fig. 5c, the inversion result of the most southern sounding of the whole campaign (sounding 1_30) shows very low resistivity at depth (about 5 Ωm). The shape of the transient gives no hint of resistive layers at depth. However, owing to the low resistivity of the layers at this site (below about 120 m depth), the investigation depth of this sounding is limited. Although the figure displays the vertical profile to a depth of some 350 m, such investigation depth cannot be reached by the measurement layout as described above given the low resistivity of the alluvial layers. From theoretical calculation it can be concluded that a resistive layer deeper than about 280 m would remain unnoticed by the TEM sounding at this point.

Groundwater flow

Figure 6 shows the piezometric surfaces of groundwater in the UKA and LKA. For the UKA, only minor manual corrections of automatically generated contour lines—mainly in areas with low measurement density—were required. Groundwater of the UKA flows in a north–south direction in the eastern parts of the ZR and in a west–east direction near the Kwando River floodplains (Fig. 6a). The latter is an indication that losing-stream conditions occur in the floodplains of the Kwando River.

The LKA appears to be confined throughout the entire area. Based on water level measurements taken in November 2015, the piezometric head in the LKA near borehole no. 041004 (Fig. 3) is over 14 m higher than in adjacent boreholes of the UKA. To the south, the measured head difference at the borehole group at site no. 200254 for the same period amounted to about 4 m. The piezometric head difference hence remains positive but gradually decreases toward the south. However, reliable groundwater contours could not be established until now. This is due to the fairly small number of boreholes, and hence limited data, and the prevailing low hydraulic gradients. In addition, most boreholes penetrate the aquifer only partially, and individual screen depths vary considerably. It is also probable that some boreholes are connected to the UKA. Despite these limitations, a general north to south flow direction could be established from hydraulic head measurements taken during November 2015 (Fig. 6a). The hydraulic gradient in this direction is estimated at 0.08 ‰.

The variable sedimentological environment, with phases of fluvial, fluvio-deltaic and lacustrine conditions, is not only responsible for the high lithological variability, but also explains the variations in hydraulic transmissivity. The box-plots shown in Fig. 6c represent the results from the available 42 single-well pumping tests. The LKA is characterized by higher transmissivity with a lower dispersion compared to the UKA. The median values of transmissivity amount to 59 m^2/d for the LKA compared to 20 m^2/d for the UKA.

Hydrochemistry

The general chemical groundwater composition exhibits strong heterogeneity, as shown in the percentile plots of Fig. 7. Due to the effects of evapoconcentration and dissolution of salts, groundwater often becomes brackish. Total dissolved solid (TDS) content of up to 600 mg/L can largely be explained by the dissolution of calcite and magnesite. Weathering of silicates also plays a role; silica content, in fact, is exceptionally high, sometimes exceeding 100 mg/L SiO_2, due to the relatively high solubility of quartz at the prevailing groundwater temperatures of >25 °C and as a result of very active CO_2 production in subtropical soils. TDS values of above 600 mg/L indicate a growing influence of evapoconcentration and/or dissolution of halite and gypsum, leading to the dominance of Na, Cl and SO_4 content in groundwater (Plata Bedmar 1999). Groundwater within or near the Kwando floodplains is generally fresh, with low TDS (median of 444 mg/L) and very low sulfate and chloride (not included in Fig. 7) content. Groundwater of this section is usually of the calcium-magnesium-bicarbonate type. Other areas show overall increased levels of sodium, chloride, sulfate and total mineral content. Boreholes in the older alluvium and in the Linyanti-Chobe swamps show extreme variations; brackish groundwater with high sulfate content is common for both areas. By contrast, the LKA shows a homogeneous composition with fair water quality (Fig. 7). Median values for TDS, sulfate and chloride are 959, 211 and 126 mg/L, respectively.

Chemical reactions such as dissolution, precipitation, ion exchange and redox reactions control and may alter the chemical composition of groundwater along the flow path. The presumed flow direction within the LKA is from the Namibian border with Zambia in the north to the border with Botswana in the south. The total flow length is approximately 80 km. The general evolution of groundwater chemistry leads from a Ca-Mg-HCO_3 to an Na-(HCO_3 + Cl + SO_4) type, as shown in the piper diagram (Fig. 8). Along the groundwater flow direction, a notable increase in TDS, chloride, sulfate and sodium content, as well as alkalinity, can be observed (Fig. 9). In contrast, calcium and magnesium content are overall very low, with values between 2 and 4 mg/L. Selected tabulated chemical analysis results obtained during this study are given in Appendix

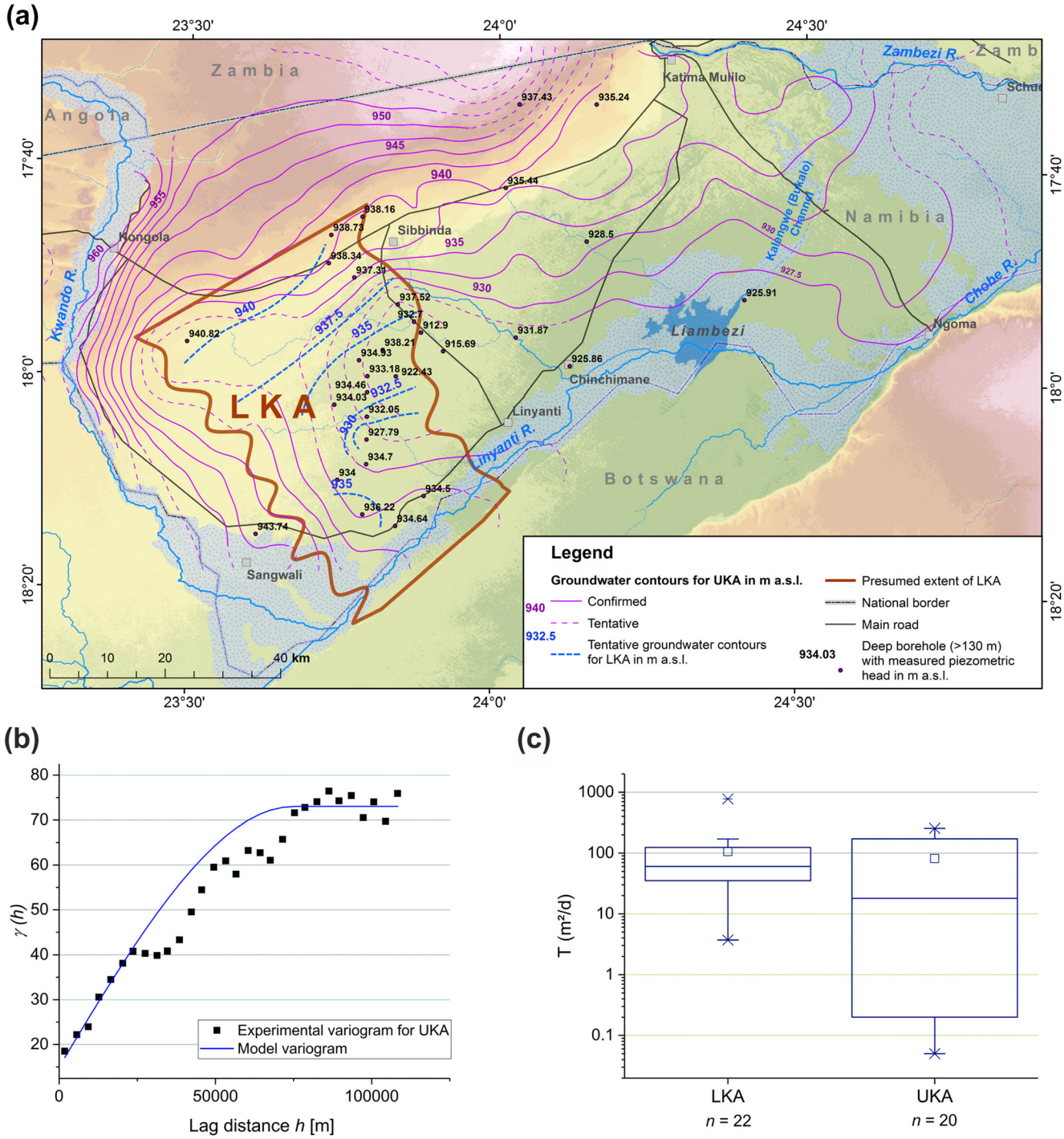

Fig. 6 **a** Piezometric surface and hydraulics of UKA and LKA in the Zambezi Region. Magenta and blue isolines denote hydraulic heads of the UKA and LKA, respectively. Broken lines show tentative contours in areas with insufficient data. **b** Variogram analysis prepared for construction of groundwater contours of UKA. Note that contours for LKA were drawn manually. **c** Box-whisker plots of transmissivity (*T*) from single-well pumping tests in the two aquifers

Table 2. Saturation indices calculated by the PHREEQC model (Parkhurst and Appelo 1999) show that the groundwater of the LKA is generally saturated with respect to calcite, magnesite and amorphous silica, and undersaturated with respect to all other major salts including gypsum, fluorspar and, obviously, halite. TDS values exceed 1500 mg/L in the southernmost areas near the Linyanti River. The correlation with flow distance is fairly strong, as shown by the Pearson product-moment correlation coefficient, *r*, of 0.88. Chloride concentrations increase from

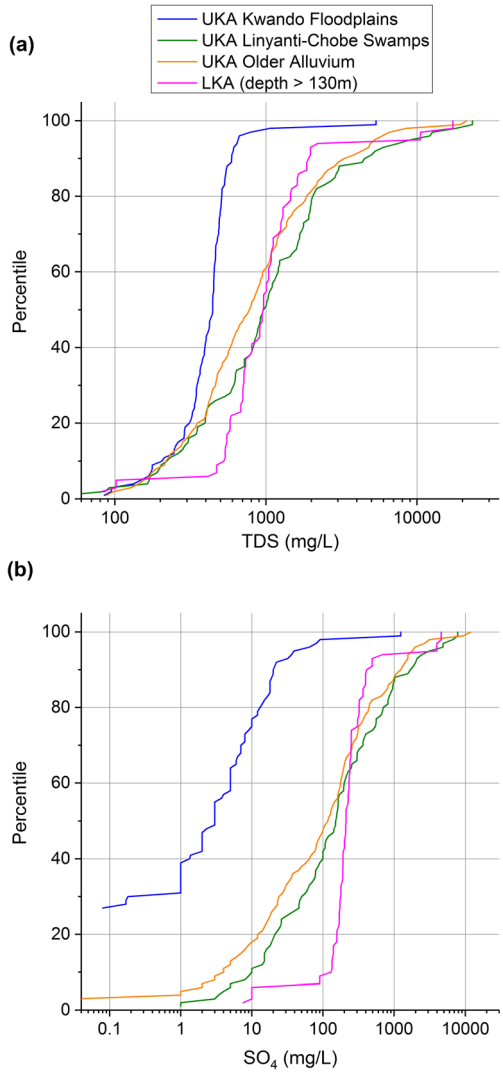

Fig. 7 Percentile plots showing **a** TDS and **b** sulfate distribution within different zones of the UKA and the LKA [data sources: Margane et al. (2005) and this study]

below 100 mg/L to over 200 mg/L, with a median of 126 mg/L. The correlation is not as strong as for TDS ($r = 0.62$) due to a significant number of outliers. Note that borehole no. 037723, whose chemistry does not seem to fit into the regional picture, is located well outside the boundaries of the known extent of the LKA (Fig. 3). Sulfate content also increases steadily ($r = 0.67$) and reaches very high levels of above 300 mg/L. The SO_4/Cl ratio (meq:meq) is on the order of 0.8–1.5, which is about 7.5–15 times that of the marine ratio of 0.104, and shows no clear trend in the N–S direction. Four rainfall samples collected at the beginning of the rainfall seasons in November 2014 and 2015, respectively, show high variations in the SO_4/Cl ratio of between 0.5 and 5.0. Unfortunately, additional data, especially during the peak of the rainy season, is not available. Although deposition of ions in bulk precipitation (precipitation + dry fallout) in windy, semi-arid environments might be higher than in humid and coastal areas, evapoconcentration of rainwater cannot explain the increase in chloride and sulfate along the flow path under confined conditions. Hence, the increase in chloride and sulfate is most likely predominantly caused by dissolution of halite and gypsum. The Br/Cl ratio can be indicative of halite dissolution. Whilst moderate evapoconcentration causes only minor changes in the Cl/Br ratio, halite dissolution may increase the value of molar Cl/Br to several thousands (Braitsch and Günter 1962). Molar Cl/Br in marine water is about 655 ± 4, and that of continental rainwater between 50 and 650 (Alcalá and Custodio 2004; Fontes and Matray 1993). Observed values in the LKA show no trend in the N–S direction and vary between 950 and 1400. They are hence indicative of moderate halite dissolution. Higher and critical (>1.5 mg/L) fluoride concentrations occur in the south of the study area. Dissolution of fluorspar facilitated by low calcium content could be one explanation; however, this would not explain the increase in fluoride toward the south, as groundwater is undersaturated with respect to fluorite throughout the area. It is therefore more likely that desorption from clay minerals—facilitated by high pH (>8.5) and competition with hydroxyl ions—is the major mechanism, as described by Jacks (2016). Sodium experiences a strong and almost uniform increase ($r = 0.81$) along the flow path, with sodium content increasing from about 50 to >600 mg/L. The Na/Cl ratio (meq:meq) remains fairly stable, with only a minor increase toward the south. The values, typically in the range of 3–4, show that halite is not the only source of sodium in the system. The increase in total dissolved inorganic carbon (TDIC) and, therefore, total alkalinity is also strongly correlated with flow distance ($r = 0.89$). Maximum values exceed 100 mg C/L. Alkalinity clearly increases by a factor of 6 to 8 at a rate of about 1.54 mg C/L per km flow distance. Furthermore, a striking correlation exists between the increase in alkalinity and in "sodium-excess", Na-Cl, defined as the molar difference between sodium and chloride in a sample. Na-Cl represents sodium that originates from sources other than halite dissolution, such as silicate weathering and ion exchange processes. The ratio of Na-Cl vs. (alkalinity + SO_4) within the LKA is almost consistently ±1, as shown in Fig. 9.

The processes that can best explain the geochemical evolution of groundwater in the LKA are cation exchange processes that consume alkaline earth metals and produce Na. The continuous removal of Ca by cation exchange along the flow path drives the progressive dissolution of calcite along the flow path and contributes alkalinity to the groundwater. In addition, sulfate is added by dissolution of gypsum. The geochemical evolution can be described by the chemical reactions:

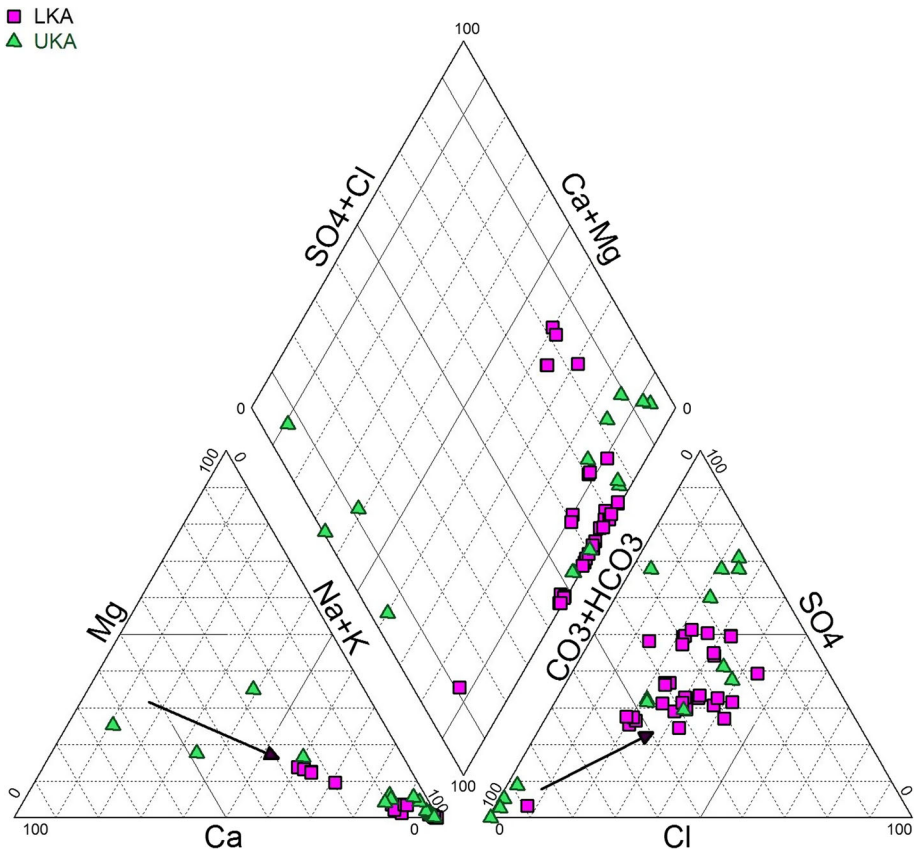

Fig. 8 Piper diagram showing the general evolution of groundwater chemistry from a Ca-Mg-HCO_3 to an Na-(HCO_3 + Cl + SO_4) type; arrows show observed trends along the flow direction

$$^{1}/_{2}Ca^{2+} + NaX \rightarrow {}^{1}/_{2}CaX + Na^{+} \quad (11)$$

$$CaCO_3 + CO_2 + CaSO_4 + 4Na{-}X + H_2O \rightarrow 4Na^{+} + 2HCO_3^{-} + SO_4^{2-} + 2Ca{-}X \quad (12)$$

and results in an Na-HCO_3-SO_4 water type. Due to the observed low redox potential, and rotten smell at some sites, there is a possibility that alkalinity is also produced by reduction of sulfate following the equation

$$SO_4^{2-} + 2CH_2O \rightarrow H_2S + 2HCO_3^{-} \quad (13)$$

However, considering the high SO_4 content in the LKA, this process is most likely of minor importance. The increase in alkalinity and the development of Na-HCO_3 water is a common phenomenon in deep-seated old groundwater, and was also reported in the Great Artesian Basin in Australia (Cresswell and Duesterberg 2012; Suckow et al. 2016), the Cretaceous sandstones of the Milk River Aquifer in Alberta, Canada (Phillips et al. 1995), and the Triassic–Cretaceous Guarani aquifer system in Brazil (Gastmans et al. 2010). Calcite is known to be abundant in the Kalahari sediments in the form of calcareous sandstone and calcrete. The prevalence of sodium as the main sorbate and the occurrence of gypsum are indicative of a more saline environment. In fact, the processes resemble that of freshening of a salty aquifer in coastal areas as described, for instance, by Appelo and Postma (2007) and van der Kemp et al. (2000). Freshening is also known to occur in aquifers within continental sedimentary basins such as the transboundary Guarani Aquifer system in South America (Houben et al. 2015; Sracek and Hirata 2002), which is composed of continental fluvial and aeolian sandstones. The Guarani Aquifer was deposited under arid conditions similar to the Northern Kalahari environment. Consequently, the system was originally brackish. It is assumed, however, that in the Guarani Aquifer, large amounts of salts may have already been flushed out after Cretaceous tectonic uplift. In contrast to the LKA, high sodium, chloride and sulfate concentrations in the center of the Guarani Basin possibly originate from mixing with water from the underlying, more saline unit or diffusion from incompletely flushed zones of lower permeability within the aquifer. What is most noteworthy about the downgradient chemical evolution observed in the LKA is that it confirms hydraulic continuity along a north–south-directed flow direction despite very low and uncertain hydraulic gradients, and provides evidence that the LKA is an

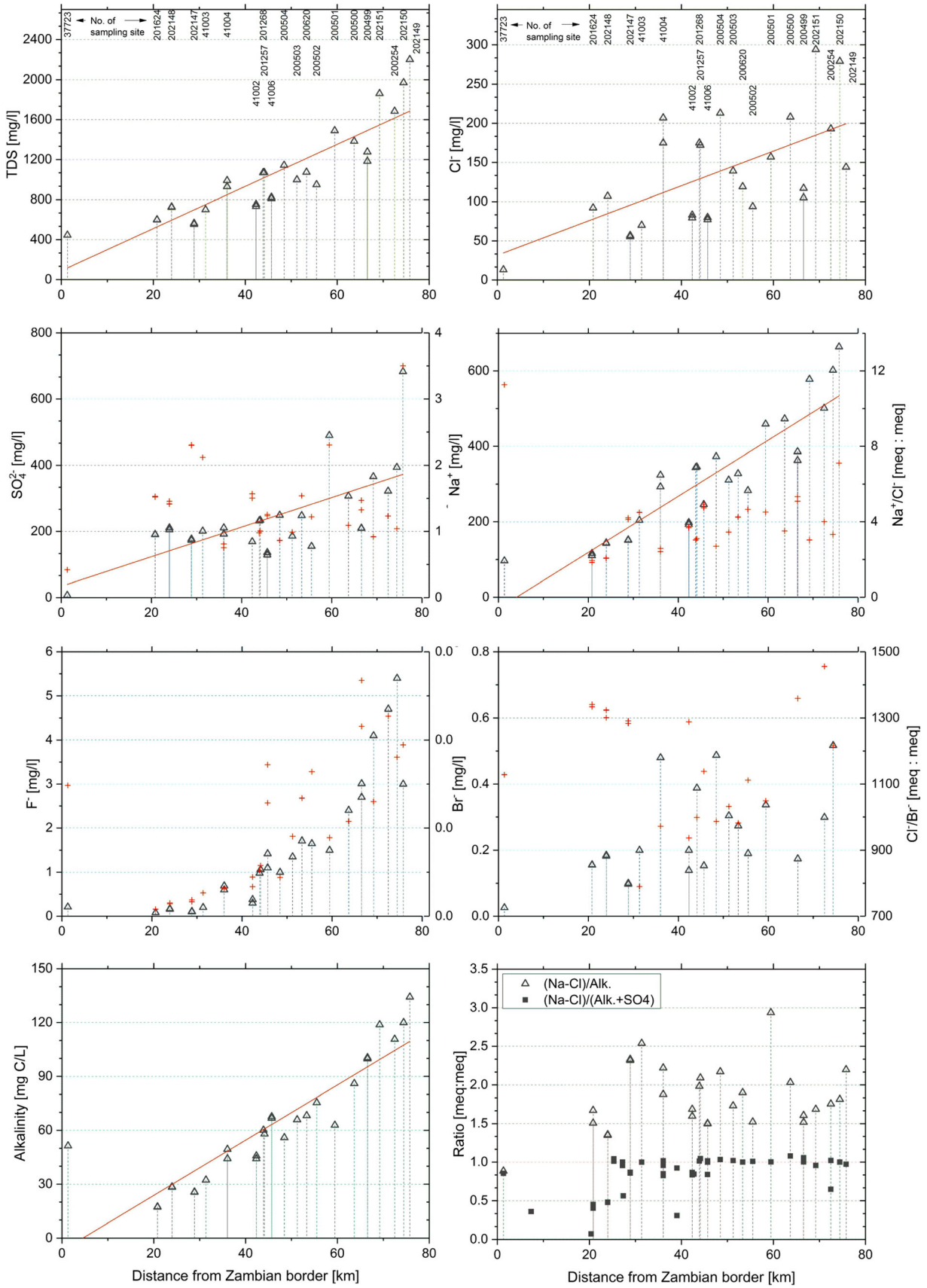

Fig. 9 Evolution of ion content and ratios in the LKA along the N–S transect. Unless otherwise stated, concentrations are represented by black hollow triangles, and ion ratios by red crosses; red lines denote trends in ion content

active hydrogeological system that still forms part of the modern hydrological cycle.

Hydro-isotopes and apparent ages

Hydro-isotope analysis results are given in Appendix Table 3. Figure 10a shows the stable isotope composition of groundwater, surface water and rainfall samples. The bulk of the samples from the LKA show the lowest observed values of deuterium and oxygen-18 of between −56 and −62 ‰ and −8.7 and −8.1 ‰ VSMOW, respectively. These samples plot near the Local Meteoric Water Line (LMWL) determined by Beyer et al. (2016) for the Ohangwena Region in northern Namibia. Four exceptions occur, namely the samples from wells no. 201624, 202147, 202148 and 041002. Their position in the diagram is clearly below the LMWL. These four wells are located in the northern margins of the known extent of the LKA (Fig. 3). Of these wells, the LKA has been properly sealed off only in well no. 041002; the screen position at boreholes no. 201624, 202147 and 202148 is 120–132 m, 90–145 m and 85–129 m, respectively (Appendix Table 2), and suggests that groundwater pumped from these wells represents mixed water from the UKA and LKA, which can explain the uncharacteristic isotope signature. Together with wells of the UKA, these samples lie near an evaporation line (EL) and are isotopically enriched due to kinetic isotopic fractionation during non-equilibrium evaporation of water. This is in good agreement with stable isotope results from previous studies in the ZR, which are shown together with the new analyses in Fig. 10b. The EL determined from all available samples follows the relationship $y = 5.47x - 12.4$ ($r = 0.99$). Samples plotting along the EL are generally characterized by low D_{ex} (Eq. (2)) of between 5 and −10 ‰, whereas most samples of the LKA have values between 7.7 and 10.3 ‰; the LKA values are closer to the D_{ex} of the local and global meteoric water, which implies that the LKA is replenished by direct recharge and fast infiltration (e.g. during storm events) and that indirect recharge from rivers or open water areas is unlikely. The orange line in Fig. 10b represents a mixing line and indicates that mixing of different groundwater with various exposure to evaporation could also, to some extent, explain the stable isotope variations. Mixing of groundwater of different age and origin may be induced by sampling boreholes with long well-screen sections which are typical for semi-arid areas like the ZR. The number of surface water samples (Fig. 10a) is insufficient for a reliable interpretation. As is to be expected, the available data also plot on an evaporation line indicative of evaporative losses; the best fit to the surface water samples shown in Fig. 10a, however, appears to differ from the EL for groundwater.

The isotope content of modern precipitation differs significantly from the characteristic low isotope content obtained for the LKA. The weighted average isotope content at climate stations of the Global Network of Isotopes (GNIP) in southern Africa is added to Fig. 10a (GNIP 2017). The Online Isotopes in Precipitation Calculator (OPIC) predicts—based on interpolation of the isotopic composition of modern meteoric precipitation—values of deuterium and oxygen-18 of −28 ± 6 ‰ and −4.6 ± 0.8‰ VSMOW for the study area (Bowen 2017; Bowen and Revenaugh 2003). The much lower values for the majority of sites from the LKA (and a noteworthy number from the UKA) could be explained by the temperature effect on isotope fractionation, a change in seasonality (i.e. from summer- to winter-dominated) or a stronger influence

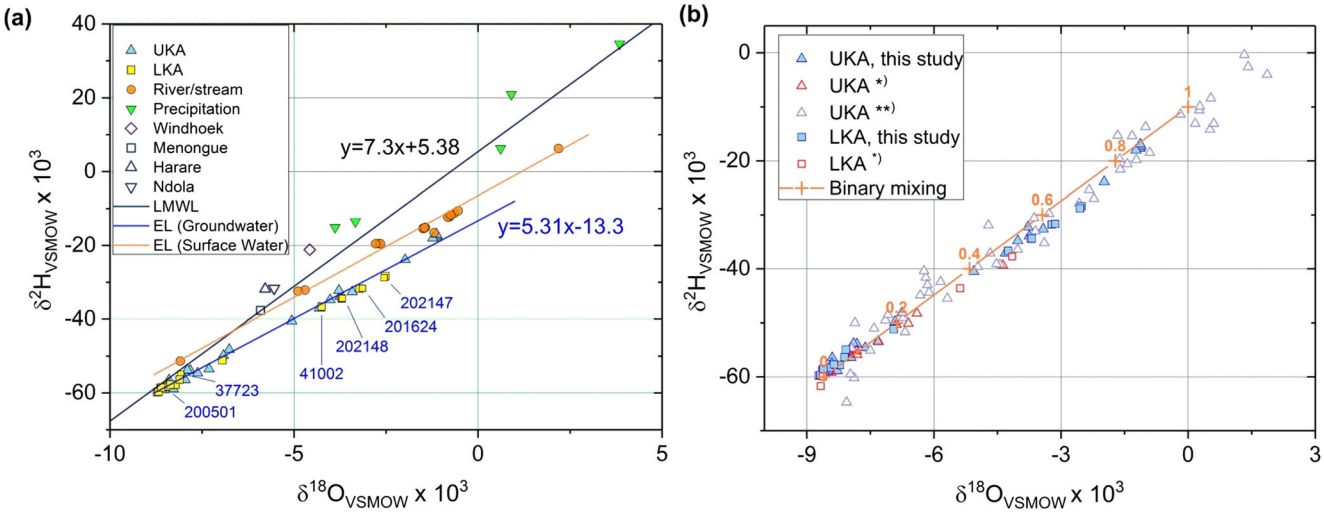

Fig. 10 **a** Stable isotope binary plots for groundwater of the UKA and LKA, surface water and precipitation. Hollow symbols represent weighted average isotope content of precipitation at selected stations in southern Africa (GNIP 2017). Local Meteoric Water Line (LMWL) after Beyer et al. (2016). **b** Comparison of groundwater stable isotope composition of this study with previous results; *data from Margane et al. (2005); **data from Plata Bedmar (1999). Numbers in orange give mixing ratios between assumed end-members

of continentality that could be produced by a change in the circulation pattern. As there is no evidence for a fundamental change in the rain-bringing climate systems in the region, the variation in average temperature is the most likely explanation. The lower isotope concentrations hence indicate that groundwater was formed under cooler than modern climatic conditions, such as during the Pleistocene, when average annual temperatures in southern Africa were about 5 °C lower than today (Holmgren et al. 2003; Kulongoski et al. 2004). The amount effect, i.e. if the percentage of high-intensity rainfall events is increased, could also contribute to lowering the $\delta^{18}O$ and $\delta^{2}H$ values of rainfall.

The bulk of the LKA samples are characterized by remarkably high ^{13}C content of between −6.6 and −4.4 ‰ VPDB and very low ^{14}C activity below 6 %mC (Fig. 11a). Exceptions are again boreholes no. 201624, 202147 and 202148, which are assumed to partially tap the UKA, with $\delta^{13}C < -11$ ‰ VPDB and ^{14}C concentrations between 30 and 42 %mC. Borehole no. 037723, which is 164 m deep but located to the northeast of the proven extent of the LKA (Fig. 3), also shows both lower ^{13}C and higher ^{14}C concentrations. Borehole no. 041002 has ^{13}C content typical of the LKA but much higher ^{14}C activity.

In an open system, the carbon-13 content of dissolved inorganic carbon in groundwater, $\delta^{13}C_{DIC}$, depends on the ^{13}C content of soil CO_2, $\delta^{13}C_{CO_2(g)}$, which is generated by the degradation of biomass, as well as pH and temperature. The pH determines the relative abundance of carbonate species $CO_{2(aq)}$, H_2CO_3,HCO_3^- and CO_3^{2-} in the water, and temperature influences the fractionation enrichment factors (e.g. Clark 2015). Common trees and bushes (*Acacia, Combretum, Sclerocarya*) near the Tswaing Crater (25°25′S, 28°5′E) show organic $\delta^{13}C_{org}$ of −30.7 to −25.5 ‰, whereas grasses and macrophytes (e.g. *Cyperaceae*) show values of −13.2 to −11.4 ‰ VPDB (Kristen et al. 2010). The lower ^{13}C content of many grasses is due to the fact that they use C4 photosynthesis, whereas most savannah trees use C3 photosynthesis. C4 plants are able to minimize water loss in hot, dry environments due to improved photosynthetic rate and efficiency, and are therefore better adapted to drier climate and lower atmospheric CO_2 concentrations (e.g. Lara and Andreo 2011; Osborne and Sack 2012). Assuming that plants using C3 photosynthesis dominate, then $\delta^{13}C_{CO_2(g)}$ typically ranges from −23 to −20 ‰ VPDB (Clark 2015). At a temperature of 28 °C, the expected $\delta^{13}C_{DIC}$ of groundwater in an open system is between −16.9 and −13.9 ‰ at pH 7, and −15.5 and −12.5 ‰ VPDB at pH 8. For a closed system, exchange with soil CO_2 is inhibited, and carbonate dissolution will reduce the initial ^{13}C content by half according to the stoichiometry of the carbonate dissolution. ^{13}C concentrations in calcretes, $\delta^{13}C_{calcrete}$, worldwide range from −14 to 4 ‰, with a maximum of −6 to −4 ‰VPDB (Talma and Netterberg 1983).

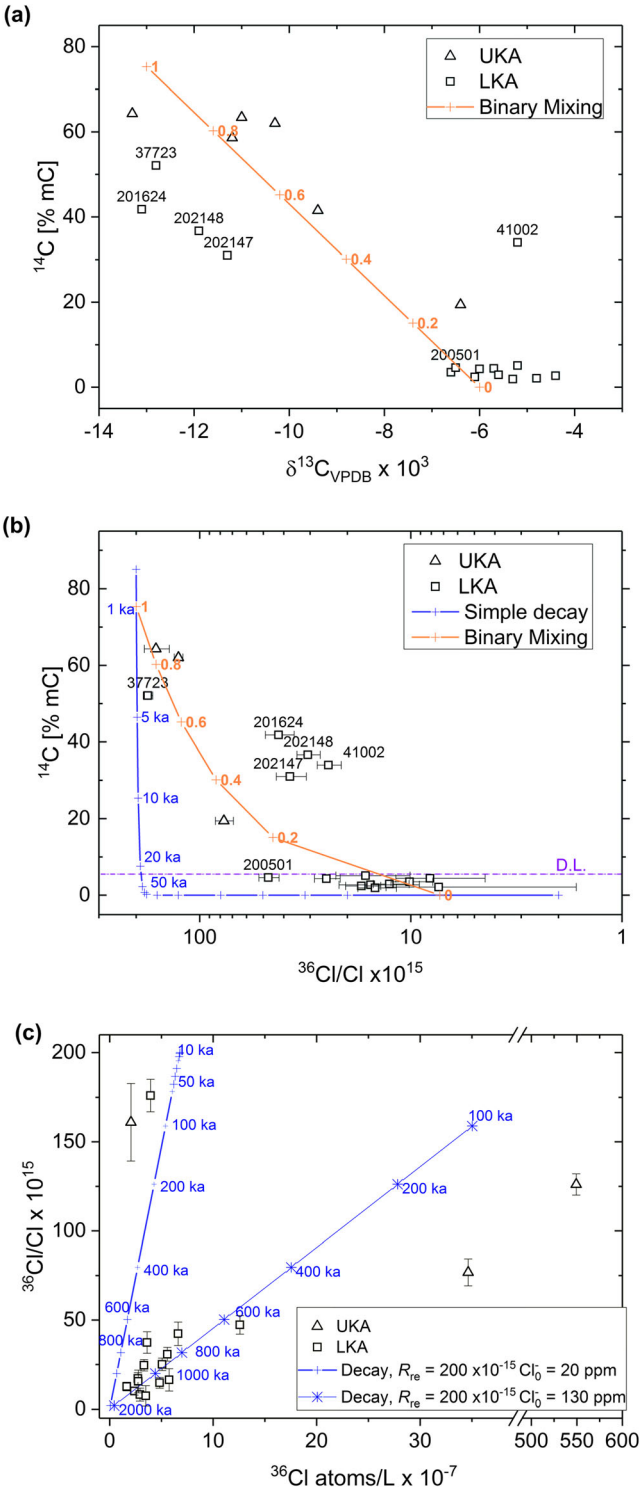

Fig. 11 Binary plots of ^{14}C concentrations vs. **a** ^{13}C concentrations, **b** $^{36}Cl/Cl$ ratio in groundwater; **c** ratio of $^{36}Cl/Cl$ ratio vs. ^{36}Cl concentration. Orange lines in graphs a and b represent binary mixing between two end-members (young and old groundwater). Blue lines in graphs b and c show ^{14}C and $^{36}Cl/Cl$, assuming simple decay and initial values of 85 %mC and 200 × 10^{-15}, respectively. D.L. = derived detection limit

Using −24 to −21 ‰ for $\delta^{13}C_{CO_2(aq)}$ and −4 ‰ for solid freshwater carbonate, the resulting $\delta^{13}C_{DIC}$ of groundwater is −14 to −12.5 ‰ VPDB, and hence in a similar range as that of an open system.

Samples from the UKA and the few outliers of the LKA samples have ^{13}C concentration similar to the values to be expected for open and closed systems. The majority of the samples from the LKA, however, have much higher values. One reason for this could be higher than presumed values of $\delta^{13}C_{calcrete}$ or a different CO_2 source. Unfortunately, sedimentary analyses of calcretes are not available in the study area. According to Talma and Netterberg (1983), soil $\delta^{13}C_{CO_2(g)}$ of −18 to −7 ‰ VPDB was measured in grassland-dominated areas of southern Africa. An abundance of C4 plants thus could be responsible for higher initial soil $\delta^{13}C_{CO_2(g)}$. Assuming soil $\delta^{13}C_{CO_2(g)}$ to be about −12 to −10 ‰ during the time of recharge of groundwater, this results in $\delta^{13}C_{DIC}$ of groundwater of −8.5 to −7.5 ‰ for closed-system conditions. For the LKA, this could mean that grassland may have prevailed during recharge. Recharge under grass-covered areas is usually higher than under densely wooded grassland, even if mean rainfall amounts are reduced due to the absence of deep-rooting trees. This observation is particularly pronounced if storm events with high rainfall intensity prevail (e.g. Kim and Jackson 2012).

Another, more likely, explanation assumes that the groundwater of the LKA is very old and the $\delta^{13}C_{DIC}$ concentrations are dominated by the carbon isotope characteristics of rock. This is because the observed progressive dissolution of carbonate associated with an increase in alkalinity and DIC steadily dilutes the original $\delta^{13}C_{DIC}$ (and ^{14}C) content. Furthermore, due to the long residence time, solute–matrix exchange occurs and groundwater DIC will approach isotopic equilibrium with carbonate rocks (e.g. Han et al. 2014). Assuming pH > 8, temperature of 28 °C and $\delta^{13}C_{calcrete}$ of −4 ‰, groundwater DIC at isotopic equilibrium with the rock matrix is enriched by about 1 ‰ compared to calcretes. The resulting value of −5 ‰ VPDB is in good agreement with measured $\delta^{13}C_{DIC}$ values. Similar effects have been observed in central parts of the Guarani Aquifer system, where dissolution of calcareous cement and isotopic exchange resulted in increased ^{13}C isotope ratios of about −6 to −8 ‰ (Gastmans et al. 2010).

Dissolution of carbonates is obvious from the observed geochemical evolution and increase in TDIC down the flow path. It is therefore tempting to assume that the very low observed ^{14}C concentrations are linked to the dissolution of dead carbon. $^{36}Cl/Cl$ ratios, however, are very low, suggesting that groundwater is much older than 50 ka and that ^{14}C must have virtually fully decayed due to its shorter half-life. This becomes obvious from the binary plot in Fig. 11b that shows the observed ^{14}C concentrations and $^{36}Cl/Cl$ ratios together with a theoretical isotope composition following simple exponential decay of the estimated respective initial concentrations. The plot can also be used to estimate the experimental detection limit for ^{14}C concentrations during this investigation, as suggested by Suckow et al. (2016). The purple horizontal line in Fig. 11b suggests that concentrations below about 5–6 %mC are affected by contamination of the samples by atmospheric CO_2 during sampling and/or analysis. This error range is plausible, as exposure of the samples to air could not be fully avoided, and CO_2 uptake is facilitated by the alkaline pH of the samples (Aggarwal et al. 2014). Mixing between older groundwater, characterized by high ^{13}C content, low $^{36}Cl/Cl$ ratios and ^{14}C of zero, with younger water of the UKA could be responsible for the different isotope content of the group of outliers within the LKA. However, as the measured values do not follow a simple binary mixing line—as indicated by the orange lines in Fig. 11—a more complex scenario involving additional end-members of mixing is apparent.

The measured $^{36}Cl/Cl$ ratios R for samples of the LKA range from 7×10^{-15} to 50×10^{-15} (atoms:atoms), with a median of 20×10^{-15}. The values for the three boreholes of the UKA and of the deep borehole 037723 located to the northeast of the LKA show significantly higher $^{36}Cl/Cl$ ratios (Fig. 11b). For three boreholes, namely 034611, 035060 and 200248, R could not be determined because the chloride concentrations of the samples were too low (i.e. <3 mg/L). The challenge in interpreting the ^{36}Cl data on the one hand is in estimating the initial $^{36}Cl/Cl$ ratios, R_{re}, as well as the secular equilibrium $^{36}Cl/Cl$ ratios in the aquifer and of a potential additional source of Cl, R_{se}. On the other hand, values of Cl vary considerably in the samples, from below 10 to 279 mg/L, which means that the origin of the Cl added after recharge needs to be clarified. The two highest measured values of R are 161 and 176×10^{-15}, which set a lower constraint to R_{re}. The uncorrected ^{14}C ages of these samples are 3651 and 9655 years, which are too low to have a significant impact on R_{re}. In published studies applying the ^{36}Cl dating technique (still a rather modest number), estimates of R_{re} are mostly between 100×10^{-15} and 500×10^{-15}. A value of 200×10^{-15}thus appears suitable for this study. R_{se} is estimated at 5×10^{-15}; this value is also similar to published data. Measured R values for the LKA are very low, and result in uncorrected apparent ages, i.e. assuming simple decay of the initial recharge concentration (Eq. (4)), of between 626 and 1433 ka. The addition of chloride could in principle be explained by variable evaporation rates in the vadose zone of the recharged water, or by addition of chloride along the flow path by dissolution of halite, mixing with brine/connate water or diffusion from adjacent aquitards. An evaporated recharge source yields a reasonable fit in a plot of R vs. the ^{36}Cl concentration, A, as shown in Fig. 11c. In this example, the average chloride concentration of LKA samples, amounting to about 130 mg/L,

was chosen as input. The identified geochemical evolution down the flow path described above and the high molar Cl/Br ratios between 950 and 1400 of groundwater from the LKA, however, suggest a different source. The average linear groundwater velocity determined by Darcy's law is 0.15 m/a applying estimates for hydraulic conductivity of 1 m/d, porosity of 0.2 and hydraulic gradient of 0.08 ‰. A value for the relative flux of chloride F of 5.9×10^9 atoms/L/a (Eq. (6)), corresponding to an addition of 3.5×10^{-4} mg/L/a of Cl, leads to an increase from an initial chloride content of 20 mg/L to about 210 mg/L at a rate of 2.3 mg/L/km over the flow distance of 80 km (Fig. 12a). Two scenarios are investigated: one in which the additional Cl is added by halite dissolution (i.e. $R_{se} = ,0$) and a second in which the chloride is added by mixing with connate water or diffusion from an aquitard ($R_{se} \neq 0$). In the first scenario, $A_{36_{Cl}}$ is unaffected but R is "diluted" by the addition of dead chlorine (Eqs. (9) and (10)). In the second case, underground production, such as by diffusion from an adjacent aquitard, adds ^{36}Cl, and with increasing time, R in the aquifer will approach secular equilibrium R_{se} (Eqs. (7) and (8)). In Fig 12, the piston-flow model (PFM) refers to simple radioactive decay of recharged ^{36}Cl in an advective transport model, ADH refers to the first scenario involving added dissolved halite, and ASC to the second scenario with an added source of ^{36}Cl by diffusion, etc. Figure 12 shows the variation in Cl, R, $A_{36_{Cl}}$ and apparent groundwater age along the presumed N–S-directed flow direction from Zambia across the study area. For the given value of R_{se}, the PFM only fits to measured $A_{36_{Cl}}$, but not R. The ADH and ASC models, in contrast, produce similar curves and appear to be suited for simulation of both R and $A_{36_{Cl}}$. The measured ^{36}Cl/Cl ratios do not decrease significantly south of about 40 km, and instead appear to approach a possible secular equilibrium (Fig. 12b). The ASC is somewhat favored over the ADH, as it is the only model in which R does not approach zero, and $A_{36_{Cl}}$ can rise with increasing time and travel distance due to underground production of ^{36}Cl (Fig. 12c). Figure 12d shows the apparent age of the samples calculated

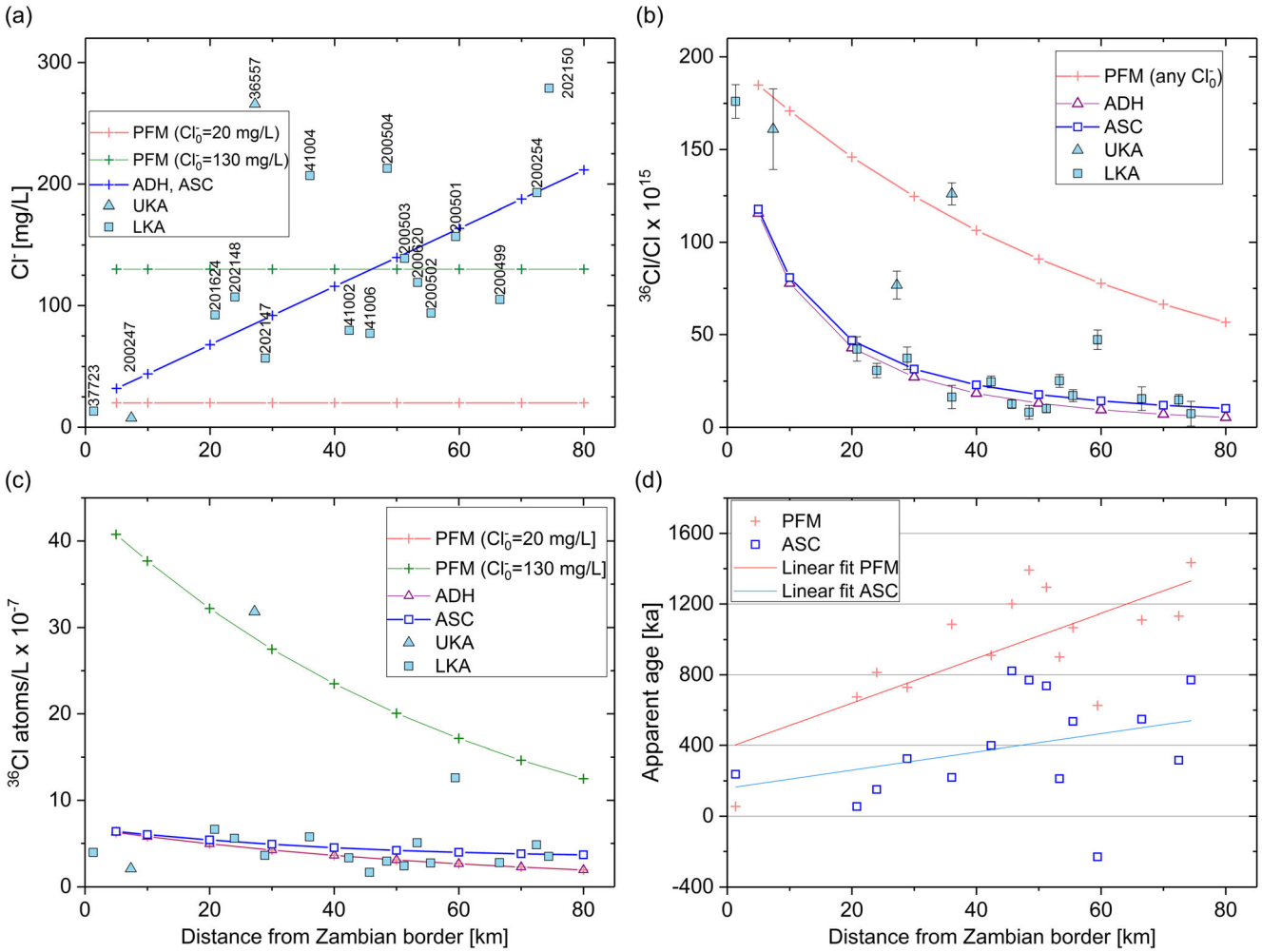

Fig. 12 Evolution of measured and simulated **a** chloride content, **b** ^{36}Cl/Cl ratio, **c** ^{36}Cl concentration [^{36}Cl atoms /L] and **d** calculated apparent groundwater ages of LKA samples along the N–S transect. For a detailed explanation and input parameters, refer to the text

for the PFM according to Eq. (4) and the ASC model according to Eq. (8). Both show a general increase in groundwater age with travel distance. The ASC produces overall lower ages because aquifer production of ^{36}Cl is superimposed on radioactive decay of recharged water. Nevertheless, ages also substantially exceed 100 ka for this model. Due to the high uncertainty on both the hydraulic and isotope input parameters, however, absolute groundwater ages cannot be determined with sufficient accuracy. At this stage, the simulations therefore are aimed at providing a better understanding of the flow and transport processes, confirming hydraulic continuity and determining coarse residence time estimates. It is quite plausible that diffusion becomes a dominant process, considering the small advective flow velocities and associated large travel times. The scatter in the data, however, implies that the overall picture is more complex and that several processes, i.e. local differences in recharge concentrations, the amount of dissolution of halite, mixing and diffusion, occur simultaneously at various degrees.

Discussion

Conceptual model

The position of the two normal Linyanti and Sibbinda faults, together with (relatively sparse) drilling information and geophysical data, reveals that the position of the top of the Karoo basalts varies significantly and abruptly, representing the tectonic structures of a rift zone. Chemical, isotope and hydraulic information indicates that the LKA represents a continuous, extremely old (i.e. >100 ka), but still active hydraulic system within this section of the ORZ. Figure 13 illustrates a conceptual model of how the aquifer system in the ZR might have developed. Accordingly, the LKA originally represents a fluvio-deltaic sedimentary sequence that was deposited prior to rifting by discharge from the northern Kwando and Zambezi rivers. With the onset of rifting associated with the formation of the ORZ—presumably from the Early to Middle Pleistocene—the LKA was tectonically displaced. Rifting

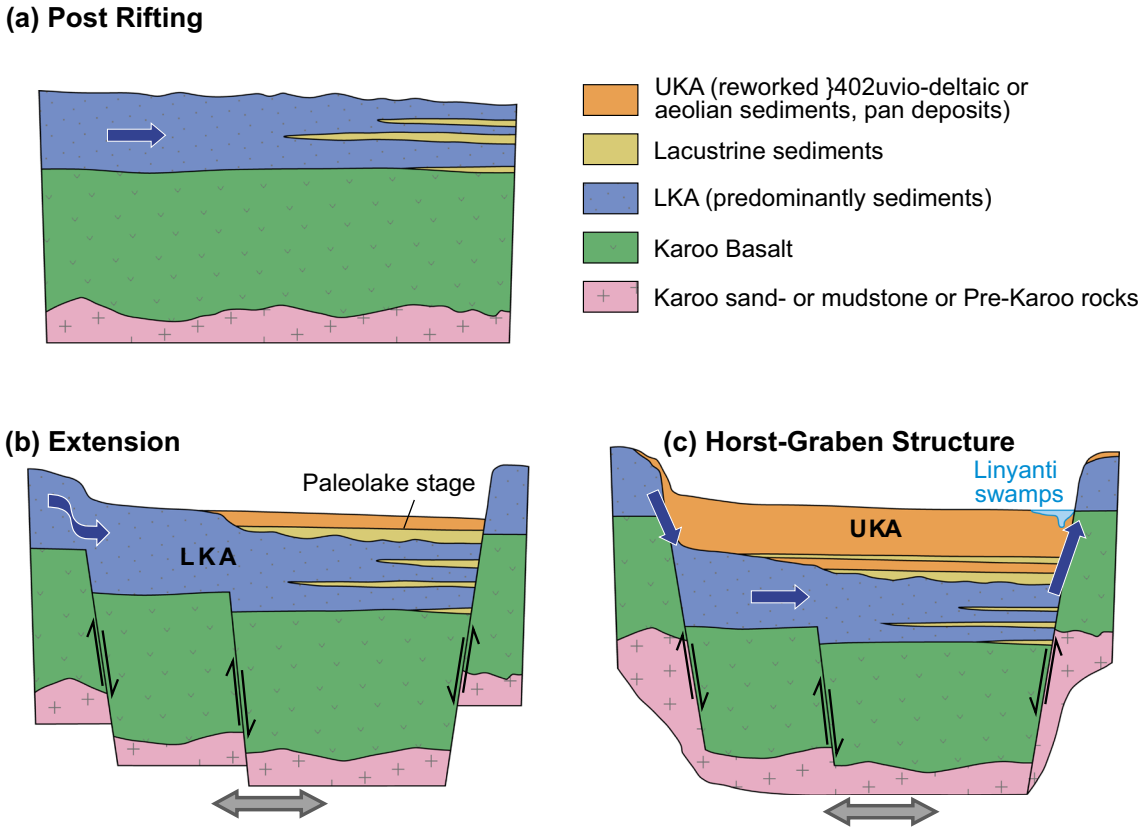

Fig. 13 Conceptual model of the development of the aquifer system in the Zambezi Region. **a** Fluvio-deltaic sediments deposited by the northern Kwando and Zambezi rivers formed the LKA prior to rifting in this area, probably during the Pliocene or early Pleistocene. **b** Extensional tectonics in the course of the formation of the ORZ—presumably during the Early to Middle Pleistocene—led to the vertical displacement of the LKA. Intermittent lacustrine phases associated with various stages of Paleolake Makgadikgadi probably extended, especially into the southern parts of the study area, thus forming clay-rich confining layers, largely burying the LKA. **c** As a result of the continuous development of the graben system in the N–S direction during the late Quaternary, the LKA was covered by younger, overall loamier deposits that form the UKA

initially occurred along the southern Chobe Fault. This led to the formation of various large paleolake stages in the Makgadikgadi Basin. The paleolake desiccated step by step due to reduction in inflow from its northern tributaries (Moore et al. 2013). Intermittent lacustrine phases probably occurred, especially in the south of the study area, thus forming clay-rich confining layers. Repeated desiccation of sections of the paleolakes led to the accumulation of evaporates within the sedimentary sequence. This explains the presence of halite and gypsum and the predominance of sodium at the cation exchange sites. With progressive extension of the graben in the N–S direction and the establishment of the Linyanti and Sibbinda faults, the LKA was further tectonically lowered and covered by younger, overall loamier deposits that form the UKA. To the north of the Sibbinda Fault, the more permeable sands of the LKA are still preserved. This area is characterized by deep-rooting Kalahari woodland. Today, a horst-graben structure is fully developed, representing more or less the final stage of tectonic evolution. The hydrochemical and isotope results provide evidence that the N–S-directed flow is still sustained, which results in a gradual freshening of a more brackish or salty groundwater system. The LKA was probably formed during the Pleistocene and recharged under colder conditions than today, with reduced evaporation. The vegetation was possibly dominated by C4 grasses or macrophytes. Modern recharge of the LKA most likely occurs along the northern graben shoulder via preferential flow through fractures and faults. In a similar way, upward-directed groundwater discharges into the Linyanti Swamps via leakage along the Linyanti Fault. Due to the low gradients and the overall reduced direct recharge under modern climate conditions, however, these processes take place very slowly.

Conclusions

The interdisciplinary investigation of the aquifers in the ZR revealed that the hydrogeological conditions are not simply controlled by modern climatic conditions, but can only be explained by considering changes in the paleoclimatic conditions and the regional tectonic history. The LKA has obviously formed under different paleoclimatic temperature, rainfall and evaporation regimes as well as vegetation cover. Subrecent and recent tectonic rifting largely controls the internal structure, extent and interlinkage with the upper aquifer. Thus, an understanding of the sedimentological and tectonic processes becomes crucial for a more effective and successful exploration and development of such an aquifer. Since characteristically little information on deep groundwater resources is available a priori—due to the risks and costs of drilling deep boreholes—the exploration of deep-seated semi-fossil or fossil aquifers should always comprise multidisciplinary research. As one of the first steps, the use of remote sensing techniques and geophysical surveys should be considered. Of particular importance are the investigation and detection of paleo-drainage conditions, hydraulic boundaries, confining layers and hydraulic windows. Subsurface geophysical data obtained from transient electromagnetic (TEM) surveys are particularly useful for detecting hydraulic boundaries as well as variations in salt content in groundwater. Hydrochemical and isotope results proved very useful in this study, as they provided additional information on groundwater flow and paleo-recharge conditions. The established geochemical evolution down the presumed flow path confirmed hydraulic continuity in a low-gradient basin. Radio-dating revealed that the age of the groundwater of the LKA is much greater than presumed, probably reaching several hundred thousands of years, implying the need for a complete set of different radioactive isotopes in order to cover the appropriate age distribution range. Challenges still exist due to insufficient data and the complex nature of recharge and groundwater flow. Stored groundwater volumes and fluxes of the LKA are still uncertain. Inflow and outflow are assumed to be minor, as modern recharge in the Kalahari Basin is very small overall. Numerical modeling based on the developed conceptual hydrogeological model could provide more insight into current groundwater discharge. Some of the available hydraulic and hydrochemical data, however, may be misleading, because most available boreholes are screened over different sections of the aquifer, and too little is known about the vertical variations in chemical properties within the aquifers. The use of radiocarbon dating in this area is limited due to rock–water interactions and because groundwater ages exceed its inherent dating limit of about 35 ka. Difficulties in dating old groundwater with ^{36}Cl have included uncertainties about the relative significance of evaporation, mixing and subsurface production in interpreting the measured variations in Cl and ^{36}Cl. The use of radioactive noble gases such as ^{39}Ar for younger groundwater near the recharge areas and ^{81}Kr for very old groundwater is very promising and could substantially improve the interpretation of available ^{14}C and ^{36}Cl data.

Acknowledgments We thank Leopold Niipare, Director of Water Supply and Sanitation Coordination in the Ministry of Agriculture, Water and Forestry of the Republic of Namibia, the Regional Office of the Directorate of Water Supply and Sanitation Coordination, and Heike Wanke and Martin Harris of the Faculty of Science at the University of Namibia for facilitating and supporting the fieldwork. We are grateful for hydrogeological data received from the Namibian Department of Water Affairs and Forestry. We would also like to thank Ms. Tania Gusse, who evaluated pumping test data during her internship at BGR, and the German Federal Ministry for Economic Development and Cooperation (BMZ) for funding the project "Investigation of Groundwater Resources and Airborne Geophysical Investigation of Selected Mineral Targets in Namibia".

Appendices

Table 2 Selected chemical in situ measurements and analysis results

ID	Site name	Date	D [a] (m)	Screen position (m)	T (°C)	pH	Eh [b] (mV)	EC (mS/m)	DO	K^+	Na^+	Mg^{2+}	Ca^{2+}	Cl^-	SO_4^{2-}	HCO_3^-	CO_3^{2-}	NO_3^-	F^-	Br^-	SiO_2	TIC [c]
									(all in mg/L)													
1	034611	20.11.15	75	n.k. [d]	26.8	6.32	−67	25.8	0.1	3.4	19.4	5.80	26.2	0.590	0.029	164	0	0.033	0.066	0.007	105	58.5
2	035060	23.11.15	99	n.k.	29.2	7.32	−63	58.8	0.02	6.2	12.2	19.6	82.4	2.40	16.6	371	0	0.004	0.509	0.015	79.5	80.0
3	036515	13.11.15	58	37–52	26.4	7.45	−111	45.1	3.55	4.6	11.0	7.71	65.2	0.923	0.079	263	0	0.057	0.225	0.004	91.7	55.8
4	036557	10.11.15	63	45–60	27.2	8.46	−60	203	0.02	4.9	433	4.64	7.10	266	349	280	0	−0.003	0.390	0.461	23.4	54.8
5	037723	13.11.15	164	n.k.	29.9	8.93	−249	44.5	0.02	1.1	96.4	2.13	8.95	13.2	7.52	245	9.1	−0.003	0.212	0.026	39.5	48.8
6	041002	20.11.15	193	125–183	29.5	8.35	−333	100	0.02	2.9	193	3.96	10.5	79.5	169	235	0	0.017	0.378	0.139	24.2	46.3
7	041004	11.11.15	222	133–215	30.5	9.28	−214	152	0.06	1.5	324	0.082	1.71	207	211	200	13.2	−0.003	0.687	0.480	19.6	39.9
8	041005	11.11.15	70	35–66	39.8	7.12	−133	2290	0.59	59.5	5725	190	162	2569	9318	1208	0	−0.003	0.855	5.28	36.8	255
9	041006	19.11.15	250	150–189	31.2	9.19	−306	99.8	0.02	2.2	246	0.174	1.41	77.1	129	305	20.8	0.018	1.42	0.153	17.9	61.9
10	200247	14.11.15	98	64–90	31.1	7.19	−107	74.1	0.85	5.1	74.0	36.6	44.9	7.54	36.9	463	0	0.237	0.328	0.029	75.7	102
11	200248	23.11.15	103	75–92	27.2	7.56	−58	46.0	0.02	4.9	65.0	9.85	23.1	2.68	6.27	290	0	−0.003	1.14	0.014	83.9	59.5
12	200254	16.11.15	200	140–195	29.2	8.88	−238	208	0.03	4.0	501	0.193	2.01	193	322	514	26.6	0.008	4.70	0.299	74.5	106
13	200499	21.11.15	190.5	162–?	29.8	9.04	−184	161	0.02	3.0	363	0.145	1.44	105	209	450	32.1	0.013	3.01	0.174	70.4	95.0
14	200501	17.11.15	182	131–176	28.7	8.89	−300	199	0.03	3.9	459	0.309	3.09	157	490	302	10.2	−0.003	1.50	0.337	39.7	59.6
15	200502	18.11.15	165	n.k.	28.8	9.15	−120	118	0.03	2.5	283	0.106	1.25	93.8	155	342	22.2	0.121	1.65	0.190	30.1	71.1
16	200503	18.11.15	178	n.k.	28.1	9.23	−221	132	0.01	2.4	311	0.147	1.45	139	186	302	17.9	0.040	1.35	0.304	23.4	61.1
17	200504	19.11.15	200	n k.	29.0	9.20	−246	160	0.01	2.4	373	0.195	2.08	213	249	258	14.3	−0.003	0.997	0.487	19.0	51.7
18	200620	21.11.15	166	n.k.	28.6	9.18	−196	151	0.02	2.4	328	0.170	1.58	119	248	313	18.3	−0.003	1.71	0.273	25.8	63.1
19	201624	12.11.15	133	120–132	31.9	8.01	−221	80.7	0.41	2.7	116	13.3	41.7	92.2	190	89.2	0	−0.003	0.082	0.156	33.6	17.8
20	202147	12.11.15	150	90–145	30.3	8.40	−64	78.4	2.16	2.1	152	2.04	13.8	56.9	177	131	0	0.022	0.102	0.100	17.1	25.6
21	202148	13.11.15	130	85–129	36.4	7.87	−69	101.9	0.19	3.3	144	14.7	47.6	107	211	146	0	0.012	0.163	0.182	33.6	29.9
22	202150	16.11.15	200	145–200	29.3	8.85	−305	255	0.02	4.5	602	0.154	1.75	279	394	564	25.5	−0.003	5.40	0.517	60.0	116

[a] D = borehole depth; [b] Eh measured against an Ag/AgCl electrode; correction for standard hydrogen electrode: +203 mV at 30 °C; [c] TIC = total inorganic carbon as mg/L carbon; [d] n.k. = not known

Table 3 Selected isotope analysis results

ID	Site name	Date	^{18}O (10^{-3} δ_{VSMOW})	ε	^{2}H (10^{-3}_{VSMOW})	ε	D_{ex} (10^{-3}_{VSMOW})	^{14}C -DIC (%mC)	ε	^{13}C -DIC (10^{-3}_{VPDB})	$^{36}Cl/Cl$ –	ε –
1	034611	20.11.15	−8.40	±0.02	−56.5	±0.1	10.7	58.6	±0.4	−11.2	too little Cl^-	–
2	035060	23.11.15	−3.78	±0.08	−32.2	±0.4	−2.0	63.4	±0.4	−11.0	too little Cl^-	
3	036515	13.11.15	−1.13	±0.09	−16.9	±0.3	−7.9	–	–	–	–	–
4	036557	10.11.15	−6.76	±0.06	−48.2	±0.3	5.9	19.4	±0.2	−6.4	7.68×10^{-14}	$\pm 7.55 \times 10^{-15}$
5	037723	13.11.15	−8.08	±0.06	−55.0	±0.1	9.7	52.1	±0.3	−12.8	1.76×10^{-13}	$\pm 9.11 \times 10^{-15}$
6	041002	20.11.15	−4.25	±0.02	−36.6	±0.2	−2.7	34.0	±0.2	−5.2	2.46×10^{-14}	$\pm 3.20 \times 10^{-15}$
7	041004	11.11.15	−8.36	±0.05	−57.7	±0.3	9.2	5.1	±0.1	−5.2	1.64×10^{-14}	$\pm 6.29 \times 10^{-15}$
8	041005	11.11.15	−7.31	±0.12	−53.5	±0.4	5.0	62.0	±0.4	−10.3	1.26×10^{-13}	$\pm 5.96 \times 10^{-15}$
9	041006	19.11.15	−8.61	±0.11	−58.5	±0.2	10.4	2.9	±0.1	−5.6	1.26×10^{-14}	$\pm 2.44 \times 10^{-15}$
10	200247	14.11.15	−8.41	±0.17	−57.5	±0.8	9.8	64.3	±0.4	−13.3	1.61×10^{-13}	$\pm 2.18 \times 10^{-14}$
11	200248	23.11.15	−6.92	±0.07	−49.8	±0.2	5.5	41.5	±0.3	−9.4	too little Cl^-	–
12	200254	16.11.15	−8.22	±0.06	−57.8	±0.1	7.9	1.9	±0.1	−5.3	1.48×10^{-14}	$\pm 3.06 \times 10^{-15}$
13	200499	21.11.15	−8.68	±0.10	−59.7	±0.3	9.7	2.7	±0.1	−4.4	1.55×10^{-14}	$\pm 6.39 \times 10^{-15}$
14	200501	17.11.15	−8.48	±0.04	−58.6	±0.1	9.3	4.6	±0.1	−6.5	4.73×10^{-14}	$\pm 5.18 \times 10^{-15}$
15	200502	18.11.15	−8.50	±0.01	−58.9	±0.1	9.1	2.4	±0.1	−6.1	1.71×10^{-14}	$\pm 3.26 \times 10^{-15}$
16	200503	18.11.15	−8.57	±0.07	−58.9	±0.4	9.7	3.5	±0.1	−6.6	1.01×10^{-14}	$\pm 2.27 \times 10^{-15}$
17	200504	19.11.15	−8.47	±0.08	−58.3	±0.2	9.5	4.4	±0.1	−5.7	8.11×10^{-15}	$\pm 3.66 \times 10^{-15}$
18	200620	21.11.15	−8.72	±0.03	−59.8	±0.3	9.9	4.3	±0.1	−6.0	2.51×10^{-14}	$\pm 3.48 \times 10^{-15}$
19	201624	12.11.15	−3.14	±0.10	−31.7	±0.1	−6.5	41.8	±0.3	−13.1	4.23×10^{-14}	$\pm 6.57 \times 10^{-15}$
20	202147	12.11.15	−2.55	±0.04	−28.8	±0.1	−8.4	31.0	±0.2	−11.3	3.74×10^{-14}	$\pm 6.07 \times 10^{-15}$
21	202148	13.11.15	−3.69	±0.08	−34.4	±0.4	−4.9	36.7	±0.2	−11.9	3.08×10^{-14}	$\pm 3.87 \times 10^{-15}$
22	202150	16.11.15	−8.11	±0.12	−56.4	±0.4	8.5	2.1	±0.1	−4.8	7.37×10^{-15}	$\pm 5.72 \times 10^{-15}$

ε standard deviation of replicate measurements

References

Aggarwal PK, Araguas-Araguas L, Choudhry M, van Duren M, Froehlich K (2014) Lower groundwater 14C age by atmospheric CO2 uptake during sampling and analysis, Groundwater 52: 20–24 https://doi.org/10.1111/gwat.12110

Alcalá FJ, Custodio E (2004) Use of the Cl/Br ratio as a tracer to identify the origin of salinity in some coastal aquifers of Spain. Paper presented at the 18th SWIM, Cartagena 2004, Spain 2004

Appelo CAJ, Postma D (2007) Geochemistry, groundwater and pollution, 2nd edn. CRC press

Baars RMT (1996) Conditions and management of the rangelands in the Western Province of Zambia. PhD Thesis, Landbouwuniversiteit Wageningen

Bentley HW, Phillips FM, Davis SD, Habermehl MA, Airey PL, Xalf GE, Elmore D, Gove HE, Torgersen T (1986) Chlorine 36 dating of very old groundwater; 1. The Great Artesian Basin, Australia. Water Resour Res 22:1991–2001. https://doi.org/10.1029/WR022i013p01991

Beyer M, Koeniger P, Gaj M, Hamutoko JT, Wanke H, Himmelsbach T (2016) A deuterium-based labeling technique for the investigation of rooting depths, water uptake dynamics and unsaturated zone water transport in semiarid environments. J Hydrol 533:627–643. https://doi.org/10.1016/j.jhydrol.2015.12.037

Bouchez A (2015) Bilan et dynamique des interactions rivières-lac(s)-aquifères dans le bassin hydrologique du lac Tchad: Approche couplée géochimie et modélisation des transferts (Assessment and dynamics of river-lake(s) interactions in the Lake Chad watershed: coupled geochemistry and transfer modeling). PhD Thesis, Aix-Marseille, Centre Européen de Recherche et d'Enseignement des Géosciences de l'Environnement

Bowen GJ (2017) The Online Isotopes in Precipitation Calculator, version 31 http://wwwwaterisotopesorg. Accessed 23 Oct 2017

Bowen GJ, Revenaugh J (2003) Interpolating the isotopic composition of modern meteoric precipitation. Water Resour Res 39. https://doi.org/10.1029/2003wr002086

Braitsch O, Günter HA (1962) Zur Bromverteilung in salinaren Salzsystemen bei 25°C (regarding the distribution of bromine in saline systems at 25°C). Die Naturwissenschaften 49:346–346. https://doi.org/10.1007/bf01185116

Bufford KM, Atekwana EA, Abdelsalam MG, Shemang EM, Atekwana EA, Mickus K, Moidaki M, Modisi MP, Molwalefhe L (2012) Geometry and faults tectonic activity of the Okavango Rift Zone, Botswana: evidence from magnetotelluric and electrical resistivity tomography imaging. J Afr Earth Sci 65:61–71. https://doi.org/10.1016/j.jafrearsci.2012.01.004

Burke K, Wilkinson MJ (2016) Landscape evolution in Africa during the Cenozoic and Quaternary—the legacy and limitations of Lester C. King. Can J Earth Sci 53:1089–1102. https://doi.org/10.1139/cjes-2016-0099

Burrough SL, Thomas DSG (2008) Late Quaternary lake-level fluctuations in the Mababe depression: Middle Kalahari palaeolakes and the role of Zambezi inflows. Quat Res 69:388–403. https://doi.org/10.1016/j.yqres.2008.02.003

Burrough SL, Thomas DSG, Shaw PA, Bailey RM (2007) Multiphase Quaternary highstands at Lake Ngami, Kalahari, northern Botswana. Palaeogeogr, Palaeoclimatol, Palaeoecol 253:280–299. https://doi.org/10.1016/j.palaeo.2007.06.010

Burrough SL, Thomas DSG, Bailey RM (2009) Mega-Lake in the Kalahari: a Late Pleistocene record of the Palaeolake Makgadikgadi system. Quat Sci Rev 28:1392–1411. https://doi.org/10.1016/j.quascirev.2009.02.007

Chase BM, Meadows ME (2007) Late Quaternary dynamics of southern Africa's winter rainfall zone. Earth Sci Rev 84:103–138. https://doi.org/10.1016/j.earscirev.2007.06.002

Chiang JCH, Friedman AR (2012) Extratropical cooling, interhemispheric thermal gradients, and tropical climate change. Ann Rev Earth Planet Sci 40:383–412. https://doi.org/10.1146/annurev-earth-042711-105545

Clark I (2015) Chapter 6: CO2 and weathering. In: Clark I (ed) Groundwater geochemistry and isotopes. CRC Press,. p 169–212

Coplen TB (2011) Guidelines and recommended terms for expression of stable-isotope-ratio and gas-ratio measurement results. Rapid Commun Mass Spectrom 25:2538–2560. https://doi.org/10.1002/rcm.5129

Cotterill FPD (2006) The evolutionary history and taxonomy of the *Kobus leche* species complex of south-central Africa in the context of Palaeo-drainage dynamics PhD Thesis, University of Stellenbosch

Cresswell RG, Duesterberg C (2012) Regional hydrogeochemistry. In: Ransley TR, Smerdon BD (eds) Hydrostratigraphy, hydrogeology and system conceptualisation of the Great Artesian Basin. CSIRO, p 191–212

de Wit M (2007) The Kalahari Epeirogeny and climate change: differentiating cause and effect from core to space. S Afr J Geol 110:367–392. https://doi.org/10.2113/gssajg.110.2-3.367

deMenocal PB, Ortiz J, Guilderson T, Adkins J, Sarnthein M, Baker L, Yarusinsky M (2000) Abrupt onset and termination of the African Humid Period: rapid climate responses to gradual insolation forcing. Quat Sci Rev 19(2000):347–361

Fanshawe DB (2010) Vegetation description of the Upper Zambezi districts of Zambia. In: Africa BF (ed) Occasional Publications in Biodiversity. Biodiversity Foundation for Africa, Bulawayo, pp 237–237

Feakins SJ, deMenocal PB (2010) Global and African regional climate during the Cenozoic. In: Lars W (ed) Cenozoic mammals of Africa. University of California Press, p 45–55

Fielitz K, Stadler C, Schildknecht F (2004) Results of time domain electromagnetic soundings and direct current soundings for groundwater exploration in three regions of NE Namibia (Interim Report) Project: Investigation of Groundwater Resources and Airborne-Geophysical Investigation of Selected Mineral Targets in Namibia. Department of Water Affairs (DWA), Namibia & Bundesanstalt für Geowissenschaften und Rohstoffe (BGR), Germany

Fontes J-C, Matray JM (1993) Geochemistry and origin of formation brines from the Paris Basin, France. 1. Brines associated with Triassic salts. Chem Geol 109:149–175

Fontes J-C, Andrews JN, Edmunds WM, Guerre A, Travi Y (1991) Paleorecharge by the Niger River (Mali) deduced from groundwater geochemistry. Water Resour Res 27:199–214

Gamrod JL (2009) Paleolimnological records of environmental change preserved on paleo-lake Mababe, Northwest Botswana. MSc Thesis, Oklahoma State University

Gärtner A, Linnemann U, Hofmann M (2013) The provenance of northern Kalahari Basin sediments and growth history of the southern Congo Craton reconstructed by U–Pb ages of zircons from recent river sands. Int J Earth Sci 103:579–595. https://doi.org/10.1007/s00531-013-0974-5)

Gasse F (2000) Hydrological changes in the African tropics since the Last Glacial Maximum. Quat Sci Rev 19(2000):189–211

Gasse F, Chalié F, Vincens A, Williams MAJ, Williamson D (2008) Climatic patterns in equatorial and southern Africa from 30,000 to

10,000 years ago reconstructed from terrestrial and near-shore proxy data. Quat Sci Rev 27:2316–2340. https://doi.org/10.1016/j.quascirev.2008.08.027

Gastmans D, Chang HK, Hutcheon I (2010) Groundwater geochemical evolution in the northern portion of the Guarani Aquifer System (Brazil) and its relationship to diagenetic features. Appl Geochem 25:16–33

GNIP (2017) Global Network of Isotopes in Precipitation (GNIP). https://nucleus.iaea.org/wiser/gnip.php. Accessed 14 Feb 2017

Grove AT (1969) Landforms and climate change in the Kalahari and Ngamiland. Geogr J 1135:191–212

Haddon IG (2005) The sub-Kalahari geology and tectonic evolution of the Kalahari Basin, southern Africa. PhD thesis. University of the Witwatersrand, Johannesburg

Haddon IG, McCarthy TS (2005) The Mesozoic–Cenozoic interior sag basins of Central Africa: the Late-Cretaceous–Cenozoic Kalahari and Okavango basins. J Afr Earth Sci 43:316–333. https://doi.org/10.1016/j.jafrearsci.2005.07.008

Han L-F, Niel Plummer L, Aggarwal P (2014) The curved 14 C vs. δ 13 C relationship in dissolved inorganic carbon: a useful tool for groundwater age- and geochemical interpretations. Chem Geol 387:111–125. https://doi.org/10.1016/j.chemgeo.2014.08.026

Heine K (1987) Zum Alter jungquartärer Seespiegelschwankungen in der mittleren Kalahari, südliches Afrika (The age of late Quaternary lake-level fluctuations in the Middle Kalahari, southern Africa). In: Coetzee JA (ed) Paleoecology of Africa and the surrounding islands. Balkema, Rotterdam, pp 73–101

Holmgren K, Lee-Thorp JA, Cooper GRJ, Lundblad K, Partridge TC, Scott L, Sithaldeen R, Siep Talma A, Tyson PD (2003) Persistent millennial-scale climatic variability over the past 25,000 years in southern Africa. Quat Sci Rev 22:2311–2326. https://doi.org/10.1016/s0277-3791(03)00204-x

Houben G, Eisenkölbl A, Dose E, Vera S (2015) The impact of high intensity no-till agriculture on groundwater quality in the subtropical Capiibary catchment, SE Paraguay. Environ Earth Sci 74:479–491

Hutchins DG, Hutton LG, Hutton SM, Jones CR, Loenhert EP (1976) A summary of the geology, seismicity, geomorphology and hydrogeology of the Okavango Delta. In: Geological Survey Department B (ed) Bulletin Series. Geological Survey Department, Botswana, Lobatse, p 26

Interpex (2016) http://www.interpex.com/ix1dv3/ix1dv3.htm, Accessed 2018

Ivester AH, Brook GA, Robbins LH, Campbell AC, Murphy ML, Marais E (2010) African palaeoenvironments and geomorphic landscape evolution: a sedimentary record of environmental change at Tsodilo Hills White Paintings Rock Shelter, Northwest Kalahari Desert, Botswana. In: Runge J (ed) Palaeoecology of Africa. CRC Press, p 53–78

Jacks G (2016) Fluoride in groundwater: mobilization, trends, and remediation. In: Thangarajan M, Singh VP (eds) Groundwater assessment, modeling, and management. CRC Press, p 339–349

Jones DL, Duncan RA, Briden JC, Randall DE, MacNiocaill C (2001) Age of the Batoka basalts, northern Zimbabwe, and the duration of Karoo Large Igneous Province magmatism. Geochem Geophys Geosyst. https://doi.org/10.1029/2000GC000110

Jourdan F, Féraud G, Bertrand H, Kampunzu AB, Tshoso G, Watkeys MK, Le Gall B (2005) Karoo large igneous province: brevity, origin, and relation to mass extinction questioned by new 40Ar/39Ar age data. Geology 33:745. https://doi.org/10.1130/g21632.1

Jourdan F, Bertrand H, Scharer U, Blichert-Toft J, Féraud G, Kampunzu AB (2007) Major and trace element and Sr, Nd, Hf, and Pb isotope compositions of the Karoo Large Igneous Province, Botswana-Zimbabwe: lithosphere vs mantle plume contribution. J Petrol 48:1043–1077. https://doi.org/10.1093/petrology/egm010

Kalin RM (1999) Radiocarbon dating of groundwater systems. In: Cook PG, Herczeg AL (eds) Environmental tracers in subsurface hydrology springer science+business media, LLC, pp 111–145

Key RM, Ayres N (2000) The 1998 edition of the national geological map of Botswana. J Afr Earth Sci 30:CD1–C25

Key RM, Mothibi D (1999) The national geological map of the Republic of Botswana. Geological Survey Department, Botswana, Lobatse

Kim JH, Jackson RB (2012) A global analysis of groundwater recharge for vegetation, climate, and Soils. Vadose Zone J 11:0. https://doi.org/10.2136/vzj2011.0021RA

Kinabo BD, Atekwana EA, Hogan JP, Modisi MP, Wheaton DD, Kampunzu AB (2007) Early structural development of the Okavango rift zone, NW Botswana. J Afr Earth Sci 48:125–136. https://doi.org/10.1016/j.jafrearsci.2007.02.005

Kristen I, Wilkes H, Vieth A, Zink K-G, Plessen B, Thorpe J, Partridge TC, Oberhänsli H (2010) Biomarker and stable carbon isotope analyses of sedimentary organic matter from Lake Tswaing: evidence for deglacial wetness and early Holocene drought from South Africa. J Paleolimnol 44:143–160. https://doi.org/10.1007/s10933-009-9393-9

Kulongoski JT, Hilton DR, Selaolo ET (2004) Climate variability in the Botswana Kalahari from the late Pleistocene to the present day. Geophys Res Lett 31:1–5. https://doi.org/10.1029/2003gl019238

Lara MV, Andreo CS (2011) C4 plants adaptation to high levels of CO2 and to drought environments. In: Shanker A, Venkateswarlu B (eds) Abiotic stress in plants - mechanisms and adaptations. InTech, Rijeka, pp 415–428

Lindenmaier F, Miller RM, Fenner J, Christelis G, Dill HG, Himmelsbach T, Kaufhold S, Lohe C, Quinger M, Schildknecht F, Symons G, Walzer A, van Wyk B (2014) Structure and genesis of the Cubango Megafan in northern Namibia: implications for its hydrogeology. Hydrogeol J 22:1307–1328. https://doi.org/10.1007/s10040-014-1141-1

Margane A, Bäumle R (2004) Groundwater investigations in the eastern Caprivi Region - evaluation of pumping tests, investigation of groundwater resources and airborne-geophysical investigation of selected mineral targets in Namibia (project no 200121376). Department of Water Affairs (DWA), Namibia & Bundesanstalt für Geowissenschaften und Rohstoffe (BGR), Germany, Windhoek, pp 48

Margane A, Beukes H (2007) Groundwater investigations in the eastern Caprivi region, phase II - 2006, investigation of groundwater resources and airborne-geophysical investigation of selected mineral targets in Namibia (project no 200124750). Department of Water Affairs (DWA), Namibia & Bundesanstalt für Geowissenschaften und Rohstoffe (BGR), Germany, Windhoek, pp 52

Margane A, Bäumle R, Schildknecht F, Wierenga A (2005) Groundwater investigations in the eastern Caprivi Region: Main hydrogeological report, investigation of groundwater resources and airborne-geophysical investigation of selected mineral targets in Namibia (project no 200124750). Department of Water Affairs (DWA), Namibia & Bundesanstalt für Geowissenschaften und Rohstoffe (BGR), Germany, Windhoek, pp 148

Margat J, Foster S, Droubi A (2006) Concept and importance of non-renewable resources. In: Foster S, Loucks DP (eds) Non-renewable groundwater resources a guidebook on socially-sustainable management for water-policy makers. UNESCO, pp 13–24

McCarthy TS (2013) The Okavango Delta and its place in the geomorphological evolution of southern Africa. S Afr J Geol 116:3–54. https://doi.org/10.2113/gssajg.116.1.1

McCarthy TS, Rubidge BS (2005) Story of earth and life. Struik Nature, Johannesburg

McFarlane MJ, Eckardt FD (2007) Palaeodune morphology associated with the Gumare fault of the Okavango graben in the Botswana/Namibia borderland: a new model of tectonic influence. S Afr J Geol 110:535–542. https://doi.org/10.2113/gssajg.110.4.535

McFarlane MJ, Eckardt FD (2008) Lake Deception: A new Makgadikgadi palaeolake. Botsw Notes Rec 38:195–201

McFarlane MJ, Eckardt FD, Ringrose S, Coetzee SH, Kuhn JR (2005) Degradation of linear dunes in northwest Ngamiland, Botswana and the implications for luminescence dating of periods of aridity. Quat Int 135:83–90. https://doi.org/10.1016/j.quaint.2004.10.025

Meier J (2008) Paläohydrogeologische und paläohydrologische Bedingungn in der Makgadikgadi Pfanne und dem Okavango Graben, Botswana (Paleohydrogeological and paleohydrological conditions in the Makgadikgadi Pan and the Okavango Graben, Botswana) MSc Thesis, Leibniz Universität Hannover [in German]

Mendelsohn J, Roberts C (1997) An environmental profile and atlas of Caprivi. Directorate of Environmental Affairs, Namibia

Miller RM (2008) The geology of Namibia. Ministry of Mines and Energy, Windhoek

Miller RM, Pickford M, Senut B (2010) The geology, palaeontology and evolution of the Eosha Pan, Namibia: implications for terminal Kalahari deposition. S Afr J Geol 113:307–334. https://doi.org/10.2113/gssajg.113.307

Modisi MP (2000) Fault system at the southeastern boundary of the Okavango Rift, Botswana. J Afr Earth Sci 30:569–578

Modisi MP, Atekwana EA, Kampunzu AB, Ngwisanyi TH (2000) Rift kinematics during incipient stages of continental extension: evidence from the nascent Okavango rift basin, northwest Botswana. Geology 28:939–942

Mook WG (2000) Environmental isotopes in the hydrological cycle, principles and applications. I. Introduction: theory, methods, review. In: Mook WG (ed) IHP technical documents in hydrology no 39, vol. I, UNESCO/IAEA, Paris

Moore AE (2004) The geomorphology of the Four Corners Area. In: Timberlake J, Childes SL (eds) AWF Four Corners TBNRM Project: Review of existing biodiversity information. Biodiversity Foundation for Africa, Harare, pp 25–66

Moore AE, Larkin PA (2001) Drainage evolution in South-Central Africa since the breakup of Gondwana. S Afr J Geol 104:47–68. https://doi.org/10.2113/104.1.47

Moore AE, Cotterill FPD, Eckardt FD (2013) The evolution and ages of Makgadikgadi palaeo-lakes: consilient evidence from Kalahari drainage evolution south-Central Africa. S Afr J Geol 115:385–413. https://doi.org/10.2113/gssajg.115.3.385

Munyikwa K, Van der Haute P, Vandenberghe D, De Corte F (2000) The age and palaeoenvironmental significance of the Kalahari Sands in western Zimbabwe: a thermoluminescence reconnaissance study. J Afr Earth Sci 30:941–956

Nicholson SE (2011) Dryland climatology. Cambridge University Press, Cambridge, U.K.

Nugent C (1990) The Zambezi River: tectonism, climatic change and drainage evolution. Palaeogeogr, Palaeoclimatol, Palaeoecol 78:55–69

O'Connor PWO, Thomas DSG (1999) The timing and environmental significance of Late Quaternary linear dune development in Western Zambia. Quat Res 52:44–55

Osborne CP, Sack L (2012) Evolution of C4 plants: a new hypothesis for an interaction of CO2 and water relations mediated by plant hydraulics. Philos Trans R Soc Lond Ser B Biol Sci 367:583–600. https://doi.org/10.1098/rstb.2011.0261

Parkhurst D, Appelo T (1999) User's guide to PHREEQC version 3 - a computer program for speciation, batch-reaction, one-dimensional transport, and inverse geochemical calculations. Denver, Colorado

Peel MC, Finlayson BL, McMahon TA (2007) Updated world map of the Köppen-Geiger climate classification. Hydrol Earth Syst Sci Discuss 4:439–473

Phillips FM (1999) Chlorine-36. In: Cook PG, Herczeg AL (eds) Environmental tracers in subsurface hydrology. Springer US, New York, pp 299–348

Phillips FM (2013) Chlorine-36 dating of old groundwater. In: Suckow A, Aggarwal PK, Araguas-Araguas L (eds) Isotope methods for dating old groundwater. IAEA, Vienna, pp 125–152

Phillips FM, Bentley HW, Davis SD, Elmore D, Swanick GB (1986) Chlorine 36 dating of very old groundwater; 2. Milk River Aquifer, Alberta, Canada. Water Resour Res 22:20003–22016. https://doi.org/10.1029/WR022i013p02003

Phillips FM, Rogers DB, Dreiss SJ, Jannick NO, Elmore D (1995) Chlorine 36 in Great Basin waters: revisited. Water Resour Res 31:3195–3204

Plata Bedmar A (1999) Groundwater investigation at Caprivi Region using isotope and chemical techniques. International Agency for Atomic Energy, Department of Water Affairs, Namibia, pp 45

Podgorski JE, Green AG, Kgotlhang L, Kinzelbach WKH, Kalscheuer T, Auken E, Ngwisanyi T (2013) Paleo-megalake and paleo-megafan in southern Africa. Geology 41:1155–1158. https://doi.org/10.1130/g34735.1

Podgorski JE, Green AG, Kalscheuer T, Kinzelbach WKH, Horstmeyer H, Maurer H, Rabenstein L, Doetsch J, Auken E, Ngwisanyi T, Tshoso G, Jaba BC, Ntibinyane O, Laletsang K (2015) Integrated interpretation of helicopter and ground-based geophysical data recorded within the Okavango Delta, Botswana. J Appl Geophys 114:52–67. https://doi.org/10.1016/j.jappgeo.2014.12.017

Pombo S, de Oliveira RP, Mendes A (2015) Validation of remote-sensing precipitation products for Angola. Meteorol Appl 22:395–409. https://doi.org/10.1002/met.1467

Railsback LB (2017) Shifts of the ITCZ with changing global temperature. http://wwwglyugaedu/railsback/FQS/FQSITCZShifts01pdf. Accessed 24 Jan 2017

Reason CJC, Landman W, Tennant W (2006) Seasonal to decadal prediction of southern African climate and its links with variability of the Atlantic Ocean. Bulletin of the American Meteorological Society 87: 941–955. https://doi.org/10.1175/bams-87-7-941

Reeves CV (1972) Earthquakes in Ngamiland. Botsw Notes Rec 4:257–261

Ridgway J, Money NJ (1981) Karroo basalts from Western Zambia and geochemical provinces in central and southern Africa. Geol Rundsch 70:868–973

Ringrose S, Huntsman-Mapila P, Basira Kampunzu A, Downey W, Coetzee S, Vink B, Matheson W, Vanderpost C (2005) Sedimentological and geochemical evidence for palaeo-environmental change in the Makgadikgadi subbasin, in relation to the MOZ rift depression, Botswana. Palaeogeogr Palaeoclimatol Palaeoecol 217:265–287. https://doi.org/10.1016/j.palaeo.2004.11.024

Robertson F (2004) Ecological Processes within the Four Corners Area. In: Timberlake J, Childes SL (eds) AWF Four Corners TBNRM Project: Review of existing biodiversity information. Biodiversity Foundation for Africa, Harare, pp 67–118

Rounds SA (2012) Alkalinity and acid neutralizing capacity (version 4.0). U.S. Geological Survey TWRI book 9, A6, 45 pp

Sahara and Sahel Observatory (OSS) (2008a) Iullemeden Aquifer System (Mali, Niger, Nigeria): concerted management of shared water resources of a Sahelian transboundary aquifer. OSS, Tunis

Sahara and Sahel Observatory (OSS) (2008b) The North-Western Sahara Aquifer System: Joint management of a transborder water basin. OeSS, Tunis

Schefuss E, Kuhlmann H, Mollenhauer G, Prange M, Patzold J (2011) Forcing of wet phases in Southeast Africa over the past 17,000 years. Nature 480:509–512. https://doi.org/10.1038/nature10685

Schneider T, Bischoff T, Haug GH (2014) Migration and dynamics of the intertropical convergence zone. Nature 513:45–53. https://doi.org/10.1038/Nature13636

Shaw PA (1988) Lakes and pans. In: Moon BP, Dardis GF (eds) The geomorphology of southern Africa. Southern Book Publishers, Pretoria, pp 120–140

Shaw PA, Thomas DSG (1988) Lake Caprivi: a late Quaternary link between the Zambezi and middle Kalahari drainage systems. Z Geomorphologie, Neue Folge 32:39–337

Shaw PA, Stokes S, Thomas DSG, Davies FBM, Holmgren K (1997) Palaeoecology and age of a Quaternary high lake level in the Makgadikgadi Basin of the Middle Kalahari, Botswana. S Afr J Sci 93:273–276

Siegfried TU (2004) Optimal utilization of a non-renewable transboundary groundwater resource – methodology, case study and policy implications. PhD Thesis, Swiss Federal Institute of Technology Zürich

Sracek O, Hirata R (2002) Geochemical and stable isotopic evolution of the Guarani Aquifer System in the state of São Paulo, Brazil. Hydrogeol J 10:643–655

Steudel T, Göhmann H, Mosimanyana E, Quintino M, Flügel W-A, Helmschrot J (2013) Okavango basin - hydrology. In: Oldeland J, Erb C, Finckh M, Jürgens N (eds) Environmental assessments in the Okavango Region – Biodiversity & Ecology 5, pp 19–22

Stokes S, Thomas DSG, Shaw PA (1997a) New chronological evidence for the nature and timing of linear dune development in the south-west Kalahari Desert. Geomorphology 137:81–93

Stokes S, Thomas DSG, Washington R (1997b) Multiple episodes of aridity in southern Africa since the last interglacial period. Nature 388:154–158

Stokes S, Haynes G, Thomas DSG, Horrocks JL, Higginson M, Malifa M (1998) Punctuated aridity in southern Africa during the last glacial cycle: the chronology of linear dune construction in the northeastern Kalahari. Palaeogeogr Palaeoclimatol Palaeoecol 137:305–322

Stone AEC (2014) Last Glacial Maximum conditions in southern Africa: are we any closer to understanding the climate of this time period? Prog Phys Geogr 38:519–542. https://doi.org/10.1177/0309133314528943

Stute M, Talma S (1997) Glacial temperatures and moisture transport regimes reconstructed from noble gas and d18O, Stampriet aquifer, Namibia. Paper presented at the IAEA international symposium on isotope techniques in the study of past and current environmental changes in the hydrosphere and the atmosphere, Vienna, 14–18 April 1997

Suckow A, Taylor A, Davies P, Leaney F (2016) Geochemical baseline monitoring, final report. CSIRO, Australia, p 59

Sultan M, Yan E, Sturchio N, Wagdy A, Abdel Gelil K, Becker R, Manocha N, Milewski A (2007) Natural discharge: a key to sustainable utilization of fossil groundwater. J Hydrol 335:25–36. https://doi.org/10.1016/j.jhydrol.2006.10.034

Sultan M, Metwally S, Milewski A, Becker D, Ahmed M, Sauck W, Soliman F, Sturchio N, Yan E, Rashed M, Wagdy A, Becker R, Welton B (2011) Modern recharge to fossil aquifers: geochemical, geophysical, and modeling constraints. J Hydrol 403:14–24. https://doi.org/10.1016/j.jhydrol.2011.03.036

Talma AS, Netterberg F (1983) Stable isotope abundances in calcretes. Geol Soc Lond Spec Publ 11:221–233. https://doi.org/10.1144/gsl.sp.1983.011.01.22

Thomas DSG, Shaw PA (1991) The Kalahari environment. Cambridge University Press, New York

Thomas DSG, O'Connor PWO, Bateman MD, Shaw PA, Stokes S, Nash DJ (2000) Dune activity as a record of late Quaternary aridity in the northern Kalahari: new evidence from northern Namibia interpreted in the context of regional arid and humid chronologies. Palaeogeogr Palaeoclimatol Palaeoecol 156:243–259

Thomas DSG, Brook G, Shaw PA, Bateman M, Haberyan K, Appleton C, Nash DJ, McLaren S, Davies FBM (2003) Late Pleistocene wetting and drying in the NW Kalahari: an integrated study from the Tsodilo Hills, Botswana. Quat Int 104:53–67. https://doi.org/10.1016/s1040-6182(02)00135-0

Unrug R (1987) Tectonic position of Karoo basalts, Western Zambia. Geophys Monogr Ser 40:319–322

USGS (2015) EarthExplorer, SRTM 1 arc-sec global data http://earthexplorer.usgs.gov/. Accessed 22 Jan 2015

USGS (2017) EarthExplorer, Sentinel-2 data http://earthexplorer.usgs.gov/. Accessed 4 Sept 2017

van der Kemp VJM, Appelo CAJ, Walraevens K (2000) Inverse chemical modeling and radiocarbon dating of palaeogroundwaters: the Tertiary Ledo-Paniselian aquifer in Flanders, Belgium. Water Resour Res 36:1277–1287

van der Lubbe JJL, Tjallingii R, Prins MA, Brummer G-JA, Jung SJA, Kroon D, Schneider RR (2014) Sedimentation patterns off the Zambezi River over the last 20,000 years. Mar Geol 355:189–201. https://doi.org/10.1016/j.margeo.2014.05.012

van der Lubbe JJL, Frank M, Tjallingii R, Schneider RR (2016) Neodymium isotope constraints on provenance, dispersal, and climate-driven supply of Zambezi sediments along the Mozambique margin during the past ~45,000 years. Geochem Geophys Geosyst 17:181–198. https://doi.org/10.1002/2015gc006080

Walford H, White N, Sydow J (2005) Solid sediment load history of the Zambezi Delta. Earth Planet Sci Lett 238:49–63. https://doi.org/10.1016/j.epsl.2005.07.014

Wallner M, Houben G, Lohe C, Quinger M, Himmelsbach T (2017) Inverse modeling and uncertainty analysis of potential groundwater recharge to the confined semi-fossil Ohangwena II Aquifer, Namibia. Hydrogeol J 25:2303–2321. https://doi.org/10.1007/s10040-017-1615-z

Wanke H (2005) The Namibian Eiseb Graben as an extension of the East African Rift: evidence from Landsat TM 5 imagery. S Afr J Geol 108:541–546

Willis KJ, Bennett KD, Burrough SL, Macias-Fauria M, Tovar C (2013) Determining the response of African biota to climate change: using the past to model the future. Philos Trans R Soc Lond Ser B Biol Sci 368:1–9. https://doi.org/10.1098/rstb.2012.0491

Yachiyo Engineering Co. Ltd. (1995) The study on the national water resources master plan in the Republic of Zambia, Final Report - Supporting Report [B] Meteorology. Japan International Cooperation Agency & Republic of Zambia, Ministry of Energy and Water Development, Lusaka, pp 1–82

Zonge (2018) Zonge International, http://zonge.com/instruments-home/instruments/. Accessed 2018